



**Master thesis on**  
**Fabrication of battery anode material from silicon nanoparticles**  
**and carbon composite by electrostatic self-assembly.**

By

Nihal Raj Shrivastava

**Supervisor**

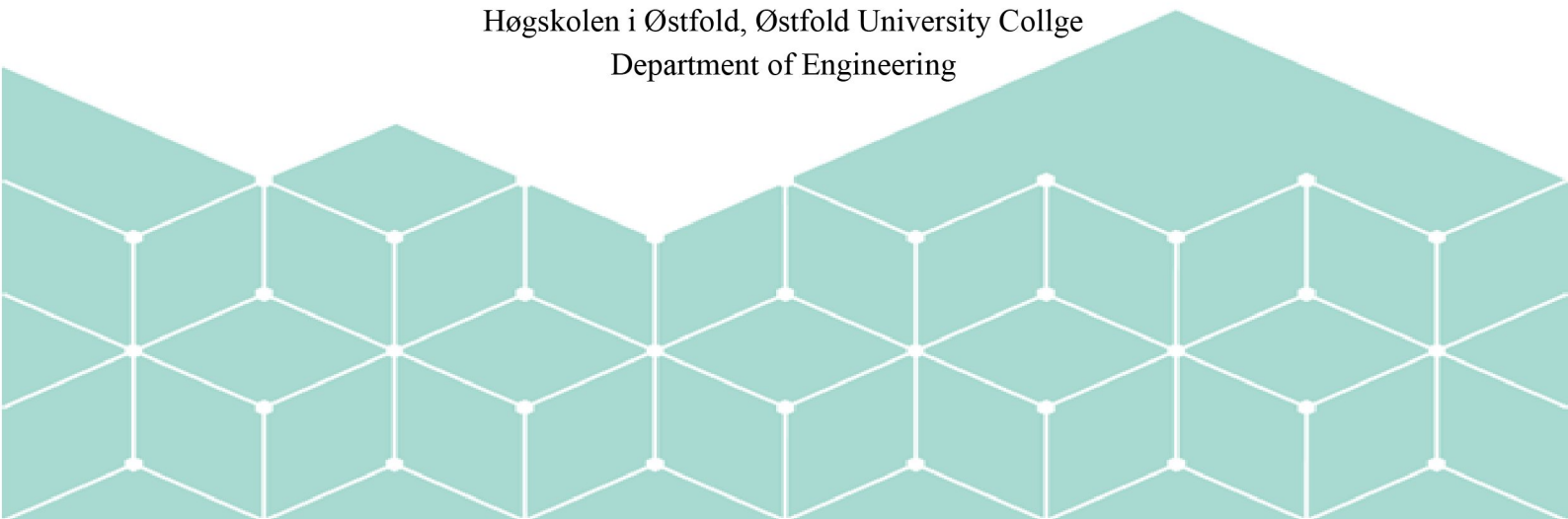
**Anna-Lena Kjøniksen**

Master in Green Energy Technology

(Materials for Energy Technology)

15.08.2023

Høgskolen i Østfold, Østfold University College  
Department of Engineering



## **Acknowledgment**

I want to take this opportunity to express my sincere appreciation to all the people whose help was an essential milestone in completing this study. This task would not have been possible without the help of a few experienced and creative people.

Most importantly, I would like to direct my sincere gratitude to my supervisor, Anna-Lena Kjøniksen, Professor, Department of Engineering at Østfold University College, whose supportive guidance improved my scientific skills.

Thanks to Sussana Saneflix, Associate Professor and course coordinator, Department of Engineering at Østfold University College, for the valuable advice and cooperation during the programme.

In addition, I am grateful to the Cartagena University and UiO for their help in conducting the tests and providing the results upon which this thesis is based.

## **Abstract**

The need of developing better and improved charge storage system is inevitable and silicon is seen as the best option for making new lithium-ion batteries because of its high specific capacity of almost 4200 mAh/g. In addition, the silicon anodes are safer to use than current system. However, using silicon in batteries has its challenges such as formation of an unstable electrolytic layer during the charge – discharge cycles and it swells and breaks during lithiation of ions.

In this research, the technique of developing Si Nanoparticles (Si NP) with carbon composite is explored. A cage of graphene which is a special kind of carbon is formed around Si NPs. This cage gives enough room for the silicon to expand making it capable to handle the stress during lithiation of ions. The graphene also forms a network in the form of Graphene nanosheet (GNS) that helps in enhancing the conductivity. This special structure makes the silicon work better in the battery.

It was found that the first charge cycle exhibited a specific capacity of 315.3 mAh/g and the first discharge cycle showed a capacity of 7.4 mAh/g which further reduced to around 2 mAh/g over 100 cycles. In addition, SEM imaging showed no presence of GNS. The battery made this way has potential to show very high specific capacity over several cycles, but the experimental technique requires appropriate composition of constituents and precise environment for assembly.

## Contents

List of abbreviations.....	5
1. Introduction .....	6
1.1. Limitation of Silicon as anode. ....	7
1.1.1. Pulverization of Silicon .....	7
1.1.2. The formation of unstable solid electrolyte interphase. ....	8
2. Inception of the idea.....	10
3. Experiment.....	12
3.1. Materials used.....	12
3.2. Synthesis of Si@SiO <sub>2</sub> . ....	12
3.3. Synthesis of Si@SiO <sub>2</sub> @GNS.....	15
3.4. Calcination and etching for structure stability. ....	15
4. Coin cell assembly.....	17
4.1. Preparing electrodes. ....	17
4.1.1. Anode.....	17
4.1.2. Cathode.....	18
4.1.3. Electrolyte. ....	19
4.1.4. Separator. ....	19
4.2. Mass loading of anode. ....	19
4.3. Assembly of 2032 coin cell. ....	20
5. Electrochemical characterization.....	22
6. Material characterization.....	24
7. Results and discussion. ....	26
8. Conclusion.....	35
9. Reference. ....	36

## List of abbreviations.

3D – Three dimensional.  
AC – Alternating current.  
aq – Aqueous.  
CMS – Carbonaceous mesophase spherules.  
CNT – Carbon nanotubes.  
CV – Cyclic voltammetry.  
DMC – Dimethyl carbonate.  
DMF – Dimethylformamide.  
EC – Electrochemical cell.  
EC – Ethylene carbonate.  
EDX – Energy dispersive X-ray spectroscopy.  
EIS – Electrochemical impedance spectroscopy.  
FTIR - Fourier Transform Infrared Spectroscopy.  
GNS – Graphene nanosheet.  
GO – Graphene oxide.  
HEMM – High-energy mechanical milling.  
ICE – Initial coulombic efficiency.  
LIB – Lithium-ion battery.  
M – Moles.  
MCMB – Mesocarbon microbeads.  
NaOH – Sodium hydroxide.  
NW – Nanowires.  
PDA – Polydopamine.  
PVC – Polyvinyl chloride  
PVDF - Polyvinylidene fluoride.  
RPM – Revolution per minute.  
SEI – Solid electrolyte interphase.  
SEM – Scanning electron microscopy.  
Si – Silicon  
Si NP – Silicon nanoparticles.  
Si NW – Silicon nanowires.  
SiC – Silicon carbon.  
TES – Trimethoxy silane.

## 1. Introduction

As the society is growing the demand of energy is also increasing. The recent instability in the world has exposed the vulnerable energy market and its dependency on fossil fuel. The fossil fuel is convenient yet imposes the threat of pollution, greenhouse effect, use of fossil fuel as arms to manipulate the world order and several other issues. These threats have motivated the society to move towards renewable sources of energy like solar, wind etc. However, one of the major challenges faced in implementation of renewable energy is its inability to be a consistent source of energy supply. The renewable source of energy is mostly dependent on natural factors like sunlight, wind which cannot be controlled and thus demands an efficient charge storage system.

Since the development of electrochemical cells, batteries have been as an integral part of charge storage eco system. Batteries are probably one of the most rapid developing technologies. The development of lithium-ion batteries (LIB) has been a game changer in the market but with rapid urge of transition of energy source to renewables, there is a demand for better and improved versions of lithium-ion batteries.

Batteries are fundamentally devices that has the capacity of storing electrical energy which is done by converting electrical energy into chemical energy and hence they are called electrochemical cell (EC). During the charge cycle of electrochemical cell, the electrical energy is stored in the form of chemical compound which later releases the stored energy in the form of an electrical current during the discharge cycle. On this basis EC is categorised as following.

- i. Primary cells – Which are designed to convert the chemical energy stored into electrical energy only once. E.g., non-rechargeable batteries.
- ii. Secondary cell – Which are designed for storing and releasing energy in a repetitive form. E.g., rechargeable batteries such as LIBs.

A typical cell reaction is dependent on two electrode reaction, one that undergoes oxidation and releases electron and another that undergoes reduction and accepts the electron as shown in figure 1.

Accordingly, the reaction at the negative electrode:



The reaction at the positive electrode:



Combining equations 1 and 2,



The opposite reaction happens in case of secondary batteries where the same amount of energy needs to be provided for charging the cell.

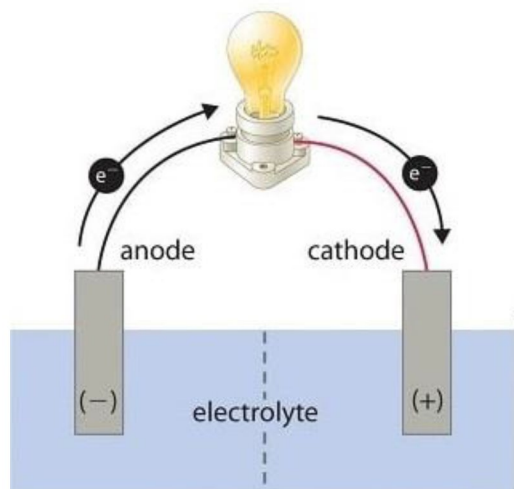
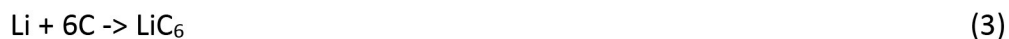


Figure 1 – Electrochemical cell. Reproduced from[2]

LIB which is a secondary cell have a typical rocking chain mechanism. During the charge cycle the Li ion gets out of lithium metal oxide ( $\text{LiMO}_2$ ) and intercalates with the graphite layer in the ratio of one lithium per six carbon as shown in equation 3 [3]. The electron flows towards the graphite because of reduction at the graphite electrode.



The opposite occurs during the discharge cycle, the lithium ion goes back to  $\text{LiMO}_2$  called deintercalation of the lithium ion. The electrons flow from the graphite electrode because of oxidation constituting the current. The electrode where oxidation and reduction takes place changes in charge and discharge cycle and that is why discharge cycle is considered conventional making anode undergoing oxidation and having negative polarity whereas cathode undergoing reduction and having positive polarity.[3]

At present graphite is generally used as the anode in a LIB which has theoretical capacity of only  $372 \text{ mAhg}^{-1}$  [4] Silicon on the other hand has received lot of attention because of its high theoretical capacity of  $4200 \text{ mAhg}^{-1}$ , low discharge potential ( $0.5 \text{ V Vs Li/Li}^+$ ) which is  $0.27 \text{ V}$  higher than graphite [3]and because of its abundant quantity in nature. [5] Despite of having many advantages, the commercial use of Silicon as an anode is currently largely restricted.

## 1.1. Limitation of Silicon as anode.

### 1.1.1. Pulverization of Silicon

One atom of Silicon can host 4 atoms of lithium [6] resulting in volume expansion of Silicon during lithiation of up to 300% [3, 4, 6]. This creates internal stress causing pulverization or

cracking of silicon (>200nm) [7] and simultaneously disconnection from the current collector resulting in low initial coulombic efficiency (ICE) as shown in figure 1. [3, 8]

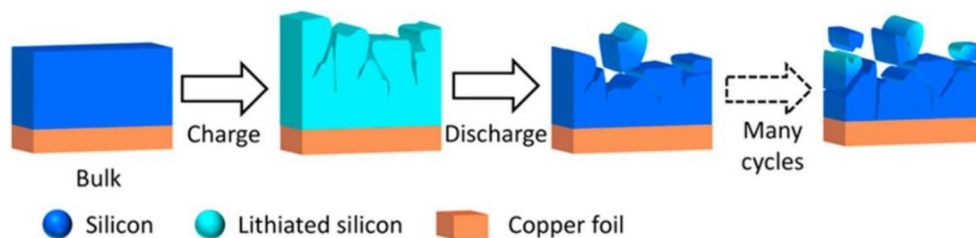


Figure 2 – Schematic diagram showing cracking of Silicon over cyclic process due to high internal stress causing disconnection from collector plate. Reproduced from [3]

To overcome the problem of pulverization many procedures has been researched such as use of Silicon nanomaterials (<50nm) in the form of nanoparticles, nano tubes, nano wires(NW), hollow spheres, and core shell structures [7]. In 2014 Xiaolin et al. [7] found that mesoporous Silicon (>20 $\mu\text{m}$ ) can control the volume expansion to close to 30%, the results were found out through combination of transmission electron microscopy and continuum media mechanical calculation. In 2012 Jin-Liang et al. [9] showed through compression simulation that during the compression phase transition of Silicon nanowires (SiNW) encapsulated in carbon nanotubes (CNT), the SiNW becomes more ductile and thus helps in overcoming the pulverization. In 2015 Wan-Jing et al. [10] observed a volume expansion of around 180% in a fully lithiated SiNP because it was encapsulated within the walls of CNT, which sustained volume expansion without fracturing its tubular structure. In 2016 Da-Eun et al. [11] studied the mechanical properties of polysaccharide binders having the effect on electrochemical performance of Si as anode in LIB. The pectin base binder provided cyclability, porosity containing the pulverization due to expansion of Si particles. The results showed that the LIB with anode made of Si and pectin binders had capacity retention of 1250  $\text{mAhg}^{-1}$  after full lithiation and at lithiation delithiation rate of 1C it showed a specific capacity of 1020  $\text{mAhg}^{-1}$  after 500 cycles in 60% by weight of Si electrode. In 2020 Xiang Guan et al. [12] researched on the synthesis of metal-chelated biomimetic polyelectrolyte binder which wraps the Si particle in a  $\text{Fe}^{3+}$ -polydopamine (PDA) layer in a thickness of 2-5nm. The  $\text{Fe}^{3+}$  forms a strong metal chelated bond with PDA providing strong mechanical strength to the protective layer and further to that the structural stability of anode increases because of 3D crosslinking structure formed due to esterification between elastic polymer and PDA. The electrochemical performance thus obtained was 2000  $\text{mAhg}^{-1}$  after 2000 cycles at 0.5C where the C is the current that would fully charge or discharge the battery in one hour. 0.5C indicates that the battery is charged at a rate of 50% of it nominal capacity per hour.

### 1.1.2. The formation of unstable solid electrolyte interphase.

The large volume expansion of Si anodes also creates problems of forming an unstable solid electrolyte interphase (SEI). SEI is a passivation layer that develops around an anode during

the first few cycles as shown in figure 3, where the SEI layer undergoes decomposition with aging becoming more porous and further getting thicker with increasing number of charge discharge cycles. Although the clear chemistry of formation of SEI is unknown, it is mostly formed due to low reduction potential ( $<1V$ ) of the anode and by electrolytic decomposition. The SEI prevents further chemical side reaction and provides long cycling life. It is not possible for LIB to undergo charge discharge reversibly without the formation of a SEI layer. SEI are electronically insulated but ionically conductive, it allows Li ions to flow through. A dense and stable SEI is an important factor for extended battery life. However, due to large volumetric expansion of Si particles the SEI layer undergoes cracking, forming exposed anode area to the electrolyte which results in formation of an extra thick SEI layer which are unstable. The unstable electrolytes result in low coulombic efficiency and higher resistance to the flow of Li ions also the thickened SEI layer increase the internal resistance of the battery. [6, 13] [14]

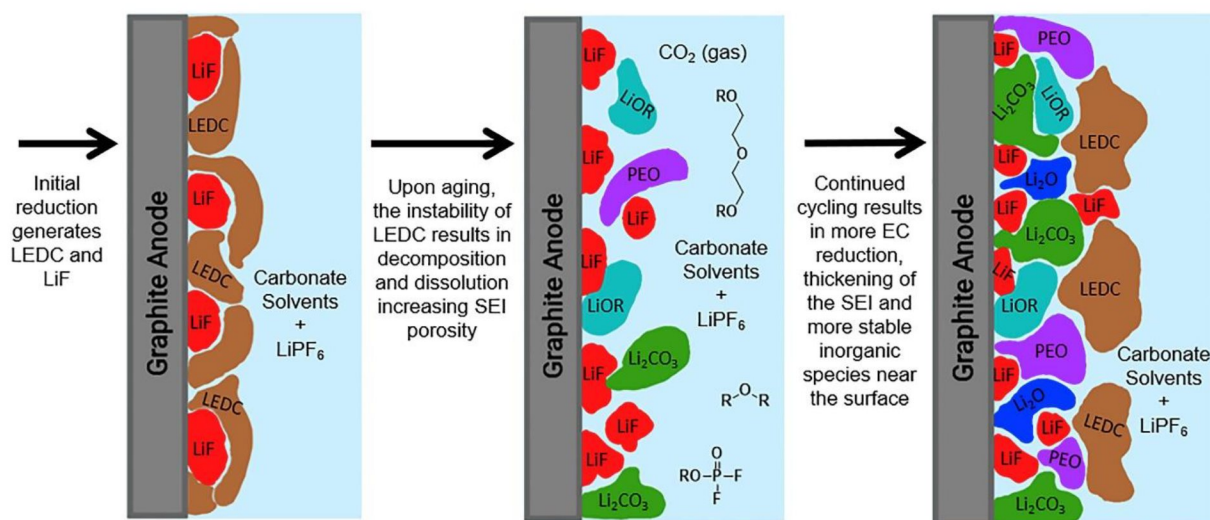


Figure 3 –The initial stage to SEI layer formation, which is then becoming porous due to decomposition upon aging, and further forming thicker layer due to more reduction. Reproduced from [13]

The use of nanotechnology has provided some breakthrough in overcoming the effect of unstable SEI layer. In 2012, Hui Wu et al. [15] experimented with Si nanotubes layered in an ion-permeable silicon oxide shell. It was found that oxide layer was protecting the outer layer of Si nanotube and the expanding inner surface almost never comes in contact of electrolyte resulting in a stable SEI. The battery showed the capacity retention of 85% over 6000 cycles of half-cell. In 2020, Yu-Ching et al. [16] researched double core-shell carbon/silicon/graphite composite anode for LIB. They chose mesocarbon microbeads (MCMB) as core material and added nano-sized Si in 30% composition on the surface with 15% of carbon coating. The capacity obtained was  $650 \text{ mAhg}^{-1}$  after 500 cycles, the capacity retention was also typically 79% with coulombic efficiency maintained at 99%. It has significant impact on stabilization of SEI as well, the impedance observed for Si/30/G/C was  $R_{\text{SEI}}=73.14 \text{ ohm}$  and for MCMB  $R_{\text{SEI}}=191.9 \text{ ohm}$ , but after making the composite the impedance was observed to be much reduced making the SEI much stable.

The above-mentioned research show that nano technology and formation of composite with carbon are proven technique to overcome the limitations faced for industrial implementation of Silicon as anode material. It was found that silicon shows particle size dependent behaviour, below 150nm there was no fracture experienced and above that the silicon particles started showing hint of pulverization and carbon being a stress buffering agent with better mechanical properties, high rate of ion flow and chemical similarity with silicon made silicon carbon composite an excellent topic to conduct research on[17].

The current research focuses on forming a graphene shell around Si nanoparticles which are then anchored on graphene sheet – SiNP@graphene shell/GNS. As shown in figure 3, the Si nanoparticle are coated with a layer of SiO<sub>2</sub> forming Si@SiO<sub>2</sub>, which is then coated with a layer of graphene oxide (GO) under electrostatic attraction. The SiO<sub>2</sub> layer is then further etched away forming an interlinked bond between Si nanoparticle with graphene shell and graphene sheet. The main objective here is eliminate the pulverization in Si particles during lithiation and delithiation so that the resulting anode when assembled in a full cell shows high specific capacity of over 1000 mAh/g over 100 charge discharge cycles.

The gap formed between Si nanoparticle and its graphene shell after etching SiO<sub>2</sub> away provides buffer space for volume expansion. The graphene sheets are known for its strength and stability which works against pulverization. The graphene sheet also boosts conductivity by interlinking the graphene shell to itself for smooth flow of Li ions throughout the anode[4].

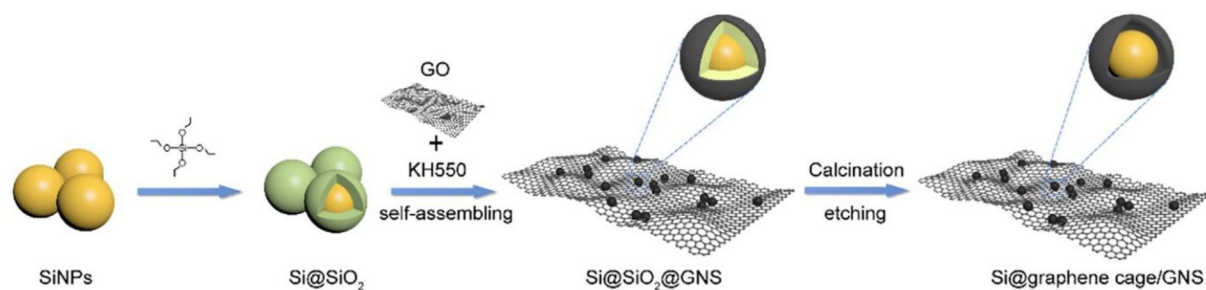


Figure 4 – Schematic showing different phase in formation of SiNP@graphene shell/GNS. Reproduced from [4]

## 2. Inception of the idea.

The preliminary investigation on the use of lithium-silicon alloys as battery anode in 1970s, when lei et al. [18] in 1976 conducted an experiment where a titanium fibre mat was impregnated with alloy of 60 wt% of Lithium and 40 wt% of Silicon at 700°C and the result showed that it was sustainable to use Lithium in higher content in the alloy as it was having higher performance potential as compared to other Li-Si alloys of different composition. Randall et al. [19] in 1977 did research on lot of Li-Si compounds like Li<sub>2</sub>Si, Li<sub>21</sub>Si<sub>8</sub> and Li<sub>15</sub>Si<sub>4</sub>

and found that 60-80% of lithium from  $\text{Li}_2\text{Si-Si}$ , over 90% of lithium from  $\text{Li}_{21}\text{Si}_8 - \text{Li}_2\text{Si}$  and 80-90% of the lithium from  $\text{Li}_{15}\text{Si}_4 - \text{Li}_{21}\text{Si}_8$  showed results at current density between 50 to 400  $\text{mA}/\text{cm}^2$  and the performance of lithium consequently did not get much affected by temperature variation. The above research was done with lithium silicon alloy in its molten form, and it was Boukamp et al. [20] in 1981 presented the concept of all solid composite electrode. The composite of finely dispersed  $\text{Li}_y\text{Si}$  in  $\text{Li}_{2.6}\text{Sn}$  was demonstrated with repetitive charge and discharge cycle without considerable loss of capacity. In 1995 Wilson et. al. [21] prepared nano dispersed silicon in carbon at 850-1050°C using chemical-vapor deposition. The X-ray absorption spectroscopy showed that silicon nanoparticles were bonded finely with carbon atoms with no large aggregation, it was assumed that there can be small aggregation of Si nanoparticles which may separate organised carbon sheets but still was believed to be a good contender of electrode for rechargeable batteries.

The late 1900 marked the beginning of research focussing on silicon nanoparticles and carbon composite for anode in rechargeable, primarily LIBs. In 1997, a technology of using Si nanoparticles as anode in LIB was patented. Hong et. al. [22] in 1999 demonstrated high reversible capacity of 1700  $\text{mAhg}^{-1}$  at 10<sup>th</sup> cycle using composite of nano silicon (70nm) powder and carbon black. Wen et. al. [23] in 2003 pyrolyzed the carbonaceous mesophase spherules (CMS) containing silicon and graphite powder to obtain silicon carbon composite samples. They found that the graphite powder (1-2  $\mu\text{m}$ ) consumed more charge for SEI film formation as a result the sample didn't show high initial efficiency expected around 74.5% but after optimization of graphite powder in the size range of 250 mesh, the result showed high efficiency of around 81% with discharge reversible capacity of 800  $\text{mAh}/\text{g}$  in initial cycles. Following Wen et al., in 2004 Liu et. al. [24] also used pyrolysis reaction of PVC (polyvinyl chloride) and silicon particles in a weight ratio of Si & PVC (3:7) following high-energy mechanical milling (HEMM). The electrode they made consist of 8 wt% acetylene black 80 wt% of active material and 12% PVDF. They concluded that temperature during synthesis has remarkable effect on electrochemical behaviour. The initial reversible capacity favoured high temperature but SiC phase got inactive around 1300°C. the result showed high coulombic efficiency of 82% and reversible capacity of 900  $\text{mAhg}^{-1}$  over 40 cycles. Pengjian et al. [25] in 2007 also used pyrolysis of a mixture of phenol formaldehyde resin, silicon powder (325 mesh) and graphite to make anode. The lithium-ion battery thus made from that anode showed a reversible discharge capacity of 700  $\text{mAhg}^{-1}$  over 40 discharge cycles.

In late 2000 the topic attracted lot of researcher's interest because of its huge potential. Some important research in the direction of encapsulating nanosized silicon core in carbon shell were, in 2008 Hyesun et. al. [26] made anode out of mesoporous Si@carbon core-shell nanowire (1D) with diameter around 6.5nm demonstrate first cycle capacity of 3163  $\text{mAhg}^{-1}$  and 87% of capacity retention after 80 cycles. In 2010 Yu Hong et. al. [27] used pyrolysis of polyvinylidene fluoride and silicon nanoparticles to form core silicon with amorphous carbon

as shell which exhibited a reversible capacity of  $1290 \text{ mAhg}^{-1}$  after 30 cycles at a current density of  $50 \text{ mA} \text{g}^{-1}$ . However, this thesis is mostly inspired by research done by Xin-Yao et al. [4] in 2019 where they used silicon nano particles as core and caged by graphene layer which were then anchored to graphene sheets as shown in figure 4. The hollow zone created between silicon core and graphene cage provided buffer to accommodate expansion and the shells anchored to graphene sheets was helpful in flow of ions as all the shells were connected to each other through graphene sheet. The reversible capacity of lithium-ion battery was demonstrated to be  $1616.1 \text{ mAhg}^{-1}$  after 100 cycles at a current density of  $1 \text{ Ag}^{-1}$ .

### 3. Experiment.

#### 3.1. Materials used.

The materials used in this experiment are described in the Table 1.

*Table 1 – Materials used in the experiment.*

Si Nanoparticles	APS<50nm, 98%, S.A. 70-100m <sup>2</sup> /g Thermo scientific
Triethoxysilane (TES)	A14965 thermoscientific.
Graphene oxide GO	796034-1G15-20 sheets Sigma-Aldrich
LiPF <sub>6</sub>	EC/DMC Sigma-Aldrich
Fluoroethylene carbonate	757349 Sigma-Aldrich
KH550 (3-Aminopropyl)triethoxysilane	281778 Sigma-Aldrich
Dimethylformaamide	A13547 thermoscientific.
Fluoroethylene carbonate	757349 Sigma-Aldrich
Toulene	28675.294 VMR Chemicals
Carbon black, acetylene	045527.30 thermoscientific

#### 3.2. Synthesis of Si@SiO<sub>2</sub>.

The different stages of synthesis of Si@graphene shell/GNS is illustrated in figure 4.

500mg of Si nanoparticles were dissolved in a mixture of 240 ml of 99% ethanol and 60ml deionised water through ultrasonication as shown in figure 5. The parameter of the ultrasonication is indicateds in Table 2.

*Table 2 – Parameter for ultrasonication procedure.*

Model	Time	Pulse	Amplitude
Qsonica Sonicators Q500	30 mins	03:03	20%

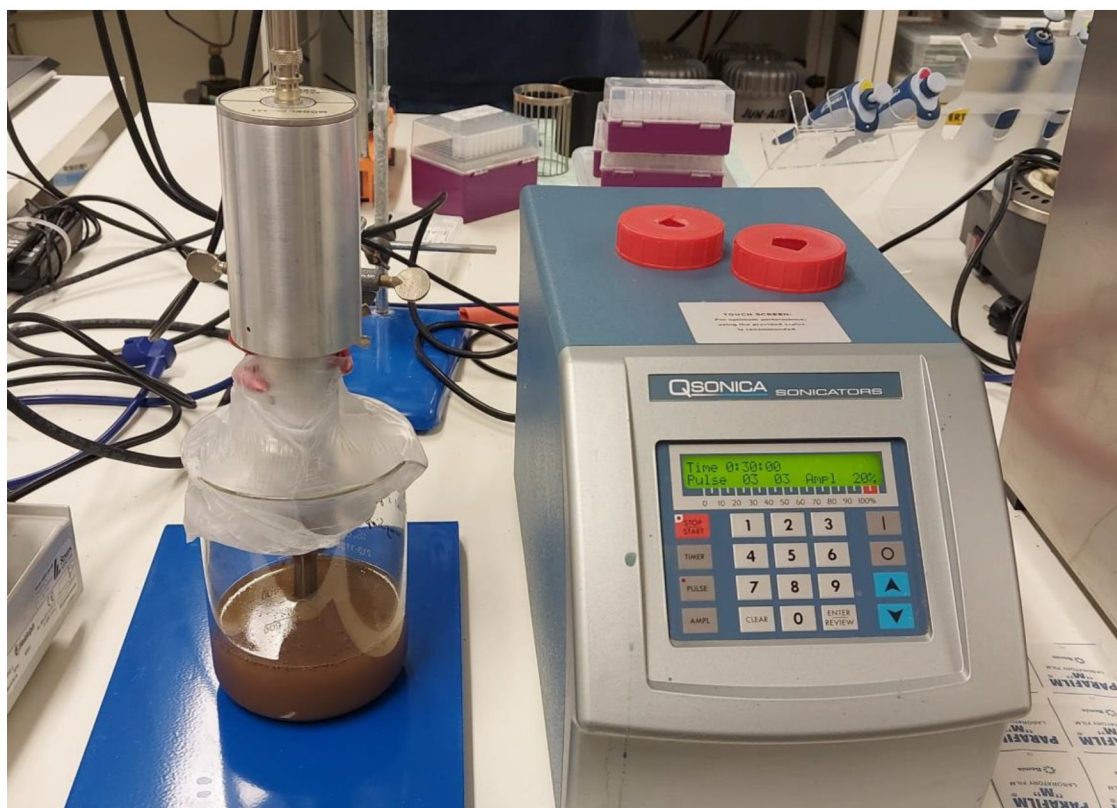


Figure 5 – Experimental picture showing ultrasonication of Si nanoparticles ethanol and deionised water.

3ml of ammonia water was then added into the Si nanoparticle solution. The solution was then kept under magnetic stirring with dropwise addition of 2.57ml of triethoxysilane (TES) over 12 hours using syringe infuser attachment as shown in figure 6 and the parameters are shown in table 3.

Table 3 – Parameters set on syringe infuser for dropwise addition of TES over 12 hours.

Model	Syringe diameter	Pumping rate	Target volume
5ml Syringe	12.5mm	0.22 ml/hr	2.57 ml

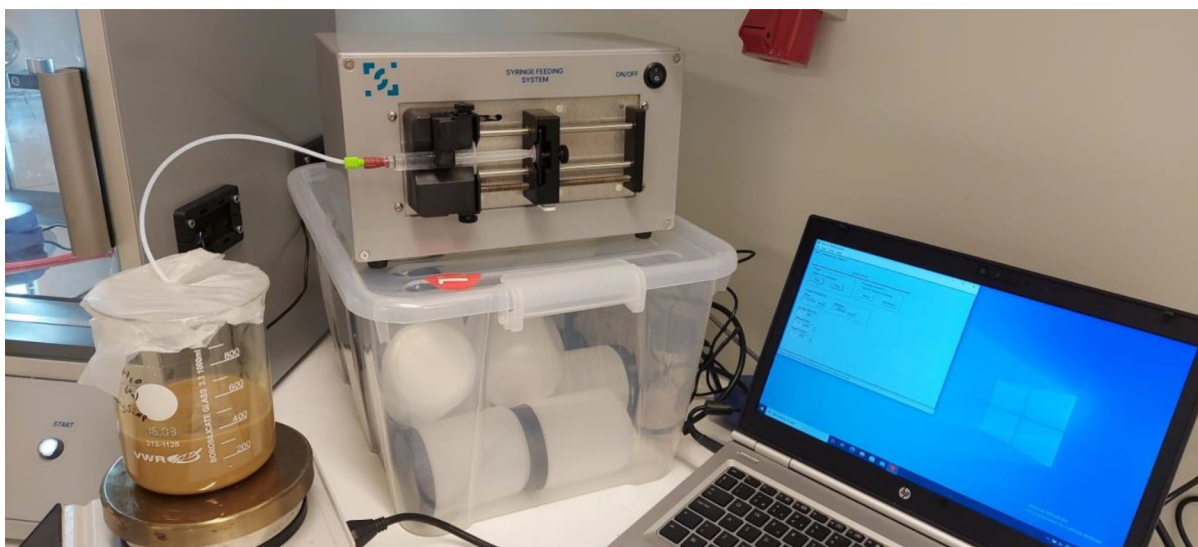


Figure 6 – Sample of Si nanoparticles on magnetic stirring with syringe infuser system injecting 2.57ml of TES over 12 hours.

The Solution of Si@SiO<sub>2</sub> was then centrifuged using the parameters in Table 4. Followed by several rounds, at least 3 times of centrifugation to wash the Si@SiO<sub>2</sub> particles thoroughly as shown in figure 7. The sample obtained was then vacuum dried at 80°C in a vacuum oven to obtain Si@SiO<sub>2</sub>.

Table 4 – Parameters for centrifuge.

Model	RPM	Time	Temperature	Acceleration	Deceleration	Bucket
VWR Mega star 1.6	4700	6 hours	24°C	5	5	3655



Figure 7 – A typical centrifuge in action.

### 3.3. Synthesis of Si@SiO<sub>2</sub>@GNS

The collected sample of Si@SiO<sub>2</sub> was then added to 50 ml of deionised water and sonicated for 30 mins using same parameter as in table 2. The same procedure was repeated for graphene oxide (GO), where 0.15 g of GO is added to 50 ml deionised water and sonicated as per Table 2 for 30 mins. Then both the aqueous solution of Si@SiO<sub>2</sub> and GO were mixed and kept on magnetic stirring at 40°C for 24 hours, a layer of GO was eventually coated over Si@SiO<sub>2</sub> under electrostatic attraction to form Si@SiO<sub>2</sub>@GNS. The solution of Si@SiO<sub>2</sub>@GNS was then vacuum filtered as shown in figure 8 using a 0.45 µm cellulose nitrate membrane filter with diameter 47mm.

The sample thus obtained was kept for drying for 2 hours at 80°C to evaporate the residual water and the dried Si@SiO<sub>2</sub>@GNS sample is obtained.



Figure 8 – Vacuum filter of Si@SiO<sub>2</sub>@GNS to drain out the water.

### 3.4. Calcination and etching for structure stability.

Calcination is the process of heating up the inorganic material at high temperature in a controlled environment to evaporate the volatile substance to avoid internal shrinkage in later stage which causes internal stress resulting in cracking or warping[28]. This technique is recognized for its ability to enhance pigment qualities such as chroma, tinctorial strength, pigmentary texture, weather stability, light-fastness, and thermal stability. However, one drawback is that it negatively impacts the dispersibility of pigments [29].

To obtain the structural stability, the dried sample Si@SiO<sub>2</sub>@GNS was kept in oven at 700°C for 2.5 hours but the sample got burned as shown in figure 9 (a).



Figure 9 – (a) The burnt sample after calcination at 700°C (b) The sample obtained after calcination at 500°C.

The calcination process was then repeated by reducing the temperature to 650, 600 and so on until the sample was properly calcinated at 500°C for 2.5 hours, the result is shown in figure 9 (b).

The calcination process was then followed by an etching process which is defined as the elimination of material from a substrate through either chemical reaction or ion bombardment [30]. Sodium hydroxide (NaOH) was utilised as etching agent here in the concentration of 2 M (2 moles of NaOH dissolved in enough water to make it 1 litre of solution) [31]. The 0.9241 g of Si@SiO<sub>2</sub>@GNS was dissolved in 129 ml of aq NaOH solution with concertation of 2M, the solution was kept on magnetic stirring for 3 hours to complete the etching process, the sample was later dried at 40°C for 2 hours. The etching removed the layer of SiO<sub>2</sub> providing space for Si NP for volume expansion as shown in figure 10 resulting is final sample which was later used as anode material.

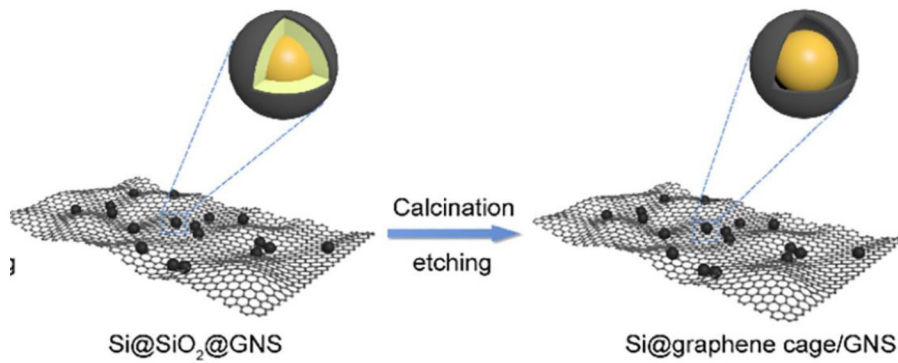


Figure 10 – Final sample anode obtained after etching. Reproduced from [4]

## 4. Coin cell assembly

### 4.1. Preparing electrodes.

The anode and cathode slurry were prepared by mixing the constituents at concentrations of [4]:

Active material (80%) + Carbon black (10%) + Binder with solvent (10%) (i)[4]

#### 4.1.1. Anode.

The active material used for the anode is the Si@graphene cage/GNS sample, which is obtained after the etching process. The preparation of the slurry involved several steps. Initially, 0.4 g of the active material were mixed with 0.05 g of carbon black. To create a suitable consistency, the mixture was combined with a 10% PVDF (polyvinylidene fluoride) solution in DMF (dimethylformamide). To enhance the liquidity of the slurry, an additional 0.3 grams of DMF was added.

The resulting solution was then subjected to a homogenizer (VMR Mixer Dig Vortex) set at 1200 rpm for a duration of 8 hours as shown in figure 11. This ensured the thorough mixing and dispersion of the components in the slurry. Once the homogenization process was completed, the slurry was cast onto a copper foil of thickness 0.25mm. The copper strip was laid on a glass plate with both ends taped with 2 layers of insulation tape and then the slurry was spread all over with the help of wooden scale getting uniform thickness. To facilitate quick drying, the casting was immediately placed on a heater at 100°C for less than 2 minutes, allowing the slurry to partially dry.



*Figure 11 – Homogenizer mixing the composition of electrodes to make slurry.*

Finally, the copper strip with the partially dried slurry was transferred to an oven and kept at 40°C for 6 hours. This controlled drying process enabled the complete solidification of the slurry, resulting in the fully casted anode on the copper strip. The carefully prepared slurry and casting procedure are vital for optimizing the performance and characteristics of the anode for its intended application.

#### 4.1.2. Cathode.

In this experiment, the cathode's active component is lithium cobalt oxide ( $\text{LiCoO}_2$ ). To create the slurry, 0.4 g of the active material and 0.05 g of carbon black are combined. This mixture is then introduced to a binder, consisting of 0.5 g of a 10% concentration PVDF solution dissolved in DMF solvent. To achieve the desired liquid consistency, an additional 0.5 g of DMF is introduced to the solution. The resulting solution is subjected to stirring on a homogenizer for a duration of 8 hours at a speed of 1200 revolutions per minute (rpm).

Subsequently, the slurry was spread evenly onto a standard aluminium foil of thickness 0.15 mm with constant thickness using same procedure as anode which is explained in section 4.1.1. This casting was then placed on a heater for approximately 2 minutes, following a procedure similar to the one employed during anode production. Following this step, the

casting was transferred to an oven and maintained at a temperature of 40°C for a duration of 6 hours resulting in fully casted cathode on copper strip.

#### 4.1.3. Electrolyte.

In this experimental setup, the electrolyte employed was a combination of LiPF<sub>6</sub> (Lithium hexafluorophosphate) with EC (ethylene carbonate) and DMC (dimethyl carbonate) that were blended within fluoroethylene carbonate. To create the electrolyte solution, a 1M concentration of LiPF<sub>6</sub> comprising 100 millilitres was mixed with EC/DMC in a specific concentration (1.0M LiPF<sub>6</sub>). Additionally, 5.25 millilitres (constituting 5% of the solution) of fluoroethylene carbonate are introduced. It's essential to emphasize that the preparation of this mixture necessitates a container that prevents light from entering, as exposure to light can induce undesirable reactions that render the mixture ineffective.

#### 4.1.4. Separator.

A Polyethylene film of thickness 0.01mm was used as separator. The separator in a battery cell is a porous membrane, which works as a physical barrier between the positive and negative electrodes. It's typically a thin and porous material that prevents direct contact between the electrodes while allowing the movement of ions. [32]

## 4.2. Mass loading of anode.

The mass loading of an electrode refers to the amount of active material that is present on the surface of the electrode. In various electrochemical applications, such as batteries, fuel cells, and capacitors, electrodes are critical components that facilitate the transfer of charge between the active material and the electrolyte. The mass loading of an electrode is an important parameter that can influence the overall performance and efficiency of the electrochemical system.

In the context of batteries, for example, the mass loading of the positive and negative electrodes (cathode and anode, respectively) can affect the energy and power density of the battery. A higher mass loading typically means more active material is available for electrochemical reactions, potentially leading to higher capacity and longer runtime. However, excessive mass loading might also lead to slower charge and discharge rates due to increased diffusion distances within the active material.

In practical applications, finding the right balance of mass loading is crucial. Too much or too little active material on an electrode can lead to suboptimal performance. Researchers and engineers work to optimize mass loading to achieve desired electrochemical performance characteristics, taking into consideration factors like energy density, power density, cycle life, and overall system efficiency.

In summary, the mass loading of an electrode is a key parameter that plays a role in determining the efficiency and performance of electrochemical systems. It's one of several factors that engineers and scientists consider when designing and optimizing such systems for various applications. [33]

In this experiment the cathode was prepared to be assembled by punching out 16 mm diameter of circular disc from the casted cathode strip of aluminium using punching tool. The weight of the cathode disc was 0.04170 g and the weight of active material of the cathode disc was 0.03337 g, the theoretical capacity of  $\text{LiCoO}_2$  is  $274 \text{ mAhg}^{-1}$  [34], and the concentration of  $\text{LiCoO}_2$  in the active material is 80 wt% (from section 4.1.2). Accordingly, the Capacity of the cathode disc = Theoretical capacity of  $\text{LiCoO}_2$  X weight of active material X  $\text{LiCoO}_2$  concentration = 7.31 mAh.

To absorb all the  $\text{Li}^+$  ions from cathode, the anode should be designed in such a way that it should match the capacity of the cathode. The theoretical capacity of silicon is  $3580 \text{ mAhg}^{-1}$  [35] the presence of Si NP in the active material is 80 wt % (from section 4.1.2). The Capacity of anode is also calculated the same way as for the cathode. To gain the same capacity of the anode like cathode, the weight of the active anode material should be 0.00255 g. The weight of the active material when the anode was taken in a square form of sides 10mm was determined to be 0.003358 g. Accordingly, the sides of the square anode should be 8.5 mm each to achieve a capacity of 7.31 mA. The cathode was therefore designed to be a circular disc of diameter 16mm and the anode was designed to be a square of each side 8.5mm, it is preferred to have anode also as a circular disc but during this experiment the punching tool was not trimming the copper sheet properly so square shape anode was cut.

According to the researcher Casper Skautvedt, at the University of Oslo, the mass per unit of anode should be between 1-5 grams/ $\text{mm}^2$ . The produced anode has 3.3 grams/ $\text{mm}^2$ , which is in the middle of desired range.

### 4.3. Assembly of 2032 coin cell.

The full 2032-coin cell assembly made with  $\text{LiCoO}_2$  active material-based cathode as positive electrode and Si@graphene cage/GNS active material as anode is shown in the general construction design as shown in figure 12.

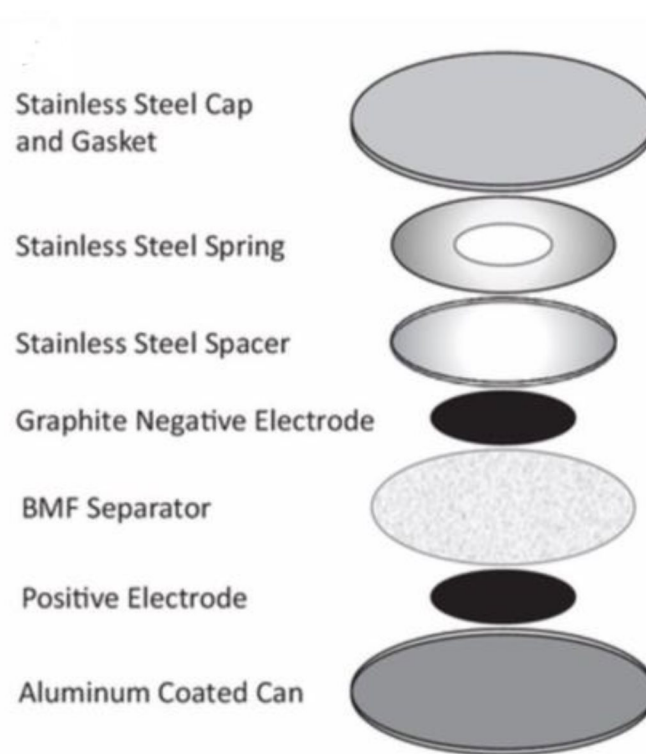


Figure 12 – Showing the general construction of coin cell assembly sequence. Reproduced from[36]

The entire assembly process was conducted within a glove box that was filled with argon gas to maintain an inert environment. Plastic tweezers were utilized to prevent any possibility of short-circuiting during the assembly process. Careful consideration was given to the arrangement of the components within the cell. To ensure the placement of the anode at the centre, the initial step involved taking the negative cap, into which a spring was inserted with its convex side facing upward. Following the spring, a stainless-steel spacer was positioned, and subsequently, the anode was delicately placed at the centre of this spacer. This was accompanied by the addition of 4 drops of electrolyte, followed by the placement of a polyethylene spacer. An additional 3 drops of electrolyte were introduced before carefully positioning the cathode, after which the positive cap of the coin cell was added.

Consequently, the cumulative mass of electrolyte dispensed amounted to 7 drops X 2.0 mg/drop, equivalent to 14 mg. With the assembly complete, the cell was meticulously lifted and positioned onto the tool post of the crimping tool as shown in figure 13. The crimping process was performed with a load that nearly reached 10 MPa or 0.5 ton, ensuring controlled and consistent sealing of the cell.[36]

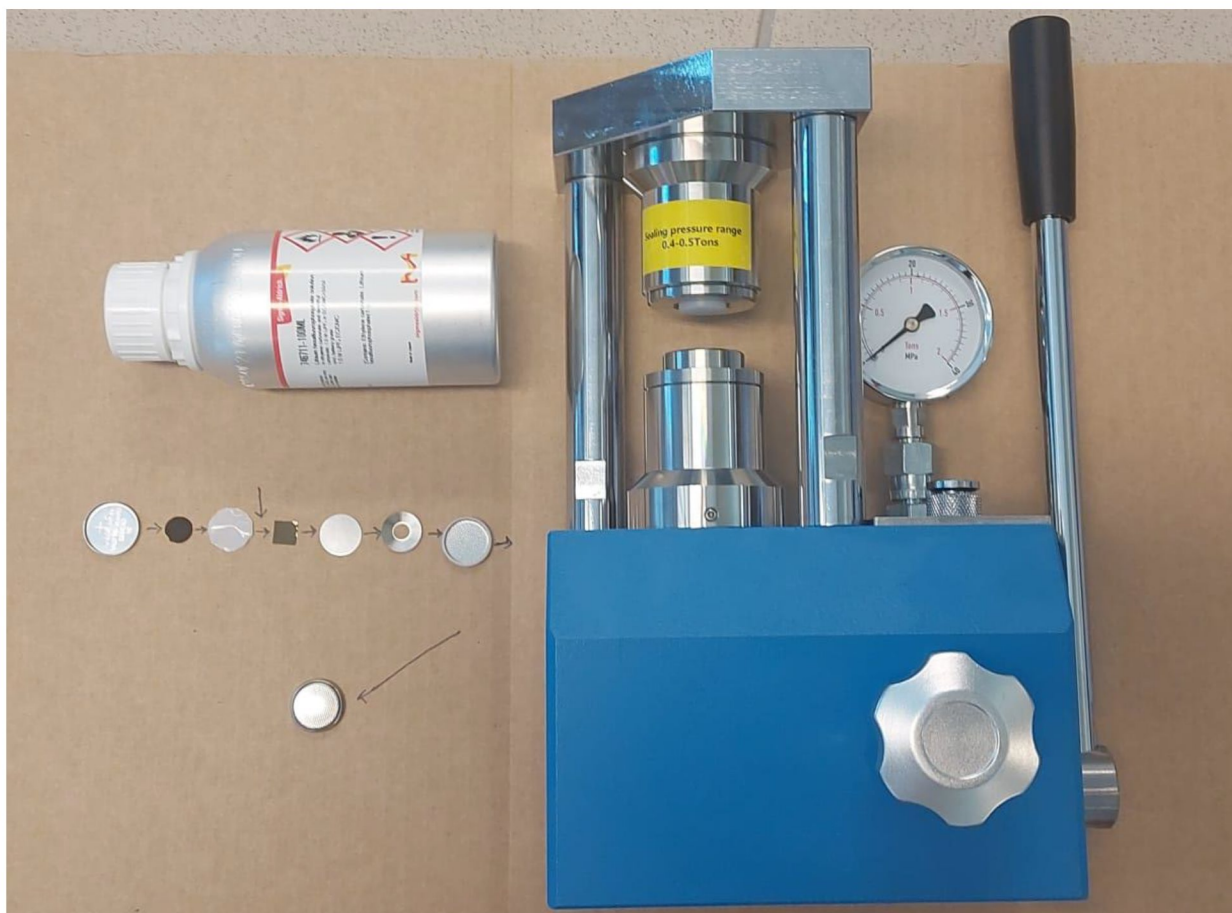


Figure 13 – Schematic showing the flow of components followed while assembly of 2032 coin cell in this experiment.

## 5. Electrochemical characterization.

Electrochemical characterization in the context of lithium-ion batteries refers to the systematic investigation and analysis of their electrochemical behaviour and performance using various experimental techniques. These techniques help researchers and engineers understand the fundamental electrochemical processes that occur within the battery during charging, discharging, and cycling. The aim of electrochemical characterization is to gather quantitative data and insights that can be used to assess the battery's efficiency, capacity, rate capability, degradation mechanisms, and other key performance parameters.

Electrochemical characterization involves applying controlled electrical signals to the battery and measuring the resulting current, voltage, or impedance responses. These measurements provide valuable information about the underlying electrochemical reactions, diffusion processes, resistance components, and overall performance of the battery. The data obtained from these experiments are then analysed to derive insights into the battery's behaviour and to optimize its design and operation.

In summary, electrochemical characterization of lithium-ion batteries encompasses a range of techniques aimed at understanding the battery's electrochemical behaviour, which is essential for improving battery performance, enhancing safety, and advancing battery technology as a whole.[37-39]

The commonly used electrochemical tests are:

i) Charge Discharge Test

A charge-discharge test, referred to as a charge-discharge cycle or cycling test, is a crucial electrochemical characterization method employed to evaluate the behaviour and performance of lithium-ion batteries. In this procedure, the battery undergoes successive phases of charging and discharging, all while closely monitoring voltage, current, and time. The objective is to assess the battery's efficiency, capacity, energy storage potential, and the possibility of deterioration across multiple cycles. [4, 37]

The charge-discharge test typically encompasses the subsequent stages:

- a) Charging phase - The battery gets connected to a power source, and a regulated current or voltage is applied to replenish its charge. During the charging process, lithium ions migrate from the cathode (positive electrode) to the anode (negative electrode), leading to energy storage.
- b) Discharging phase - Once the battery is completely charged or attains a desired state of charge, the power source disconnects, and the battery undergoes discharging. Throughout discharging, the stored energy is released as lithium ions travel from the anode to the cathode.
- c) Cycling - The charge-discharge cycle is repeated numerous times to evaluate real-world battery use. This repetition aids in evaluating the battery's capacity stability for capacity reduction, and prolonged performance.

Charge-discharge tests are essential to figure out if lithium-ion batteries are right for certain tasks. These tests help us understand how well the battery can store and give out energy, handle different levels of charging and using up energy, and work in different situations.

ii) Cyclic Voltammetry

In Cyclic Voltammetry (CV), a potential waveform is applied to the battery and the resulting current is measured. This technique helps to understand the redox reactions and electrochemical behaviour of the battery materials. Cyclic voltammetry is like taking a battery and gently pushing its energy levels up and down, while watching how it responds. It helps us understand how the battery's parts interact and how they change when we charge and discharge the battery in a controlled way. This can give us insights into how good the battery is at storing and releasing energy. [4, 37, 40-42]

### iii) Coulombic efficiency measurement

The battery's coulombic efficiency and potential losses can be determined by monitoring the ratio of discharged charge to charged charge over cycles. Coulombic efficiency is measuring how well a battery is working when you charge and discharge it. It tells you how much of the energy you put into the battery during charging can actually be taken out during discharging.

### iv) Electrochemical Impedance Spectroscopy

Electrochemical Impedance Spectroscopy (EIS) involves applying an AC voltage signal and measuring the resulting current response over a range of frequencies. It is used to analyse the battery's impedance behaviour and provides information about internal resistance and diffusion processes. It also helps in understanding the aging effect of LIB.[42, 43]

In this study, an assessment was carried out using a charge-discharge cycle test, and the data concerning coulombic efficiency were examined. The constructed 2032-coin cell underwent testing within a voltage span of 1 to 2 volts versus a lithium reference electrode (Li/Li+). The current was drawn out at a rate of 0.24mA while considering 100mA/g of the active material. The experiment involved subjecting the assembled coin cell to these specific conditions to analyse its performance.

## 6. Material characterization.

Material characterization of lithium-ion batteries involves examining and understanding the properties, structures, and behaviours of the different components that make up the battery. These components include electrode materials (cathodes and anodes), electrolytes, separators, and any other materials used in the battery's construction. The thorough investigation these materials provides insights into how they interact, react, and influence the overall performance and longevity of the battery. The material characterization aims to achieve following goals.

### i) Identify chemical and physical properties.

SEM (Scanning electron microscope), Energy Dispersive X-ray Spectroscopy (EDX) techniques are used to determine the chemical composition, crystal structure, and surface morphology of the materials.

### ii) Analyse Microstructure

This reveals information about the particle size, distribution, porosity, and interface which helps in optimizing energy storage and transfer within the battery.

### iii) Assess thermal and mechanical properties.

This helps in determining how materials respond to temperature change and mechanical stress. These insights are vital for predicting battery safety and durability.

iv) Evaluating degradation mechanism

Long-term studies and analyses of battery materials reveal degradation mechanisms, such as the growth of solid-electrolyte interface (SEI) layers on electrode surfaces, shedding light on the factors causing battery aging.

Ultimately, material characterization is fundamental to enhancing the efficiency, safety, and lifespan of lithium-ion batteries, driving advancements in energy storage technology. [39, 42, 44].

The 3<sup>rd</sup> batch of resulting sample (0.07 grams) of Silicon NP and 4<sup>th</sup> batch sample (0.088 grams) Silicon microparticles (325mesh) was sent to University Cartegena for testing morphology of samples using following techniques.

i) Raman analysis

Raman spectroscopy is a powerful analytical technique used to study the molecular composition and vibrational modes of materials. It provides insights into the unique vibrations of molecules and helps identify chemical compounds, determine molecular structures, and understand interactions between atoms in a substance. The Raman spectroscopy takes place in following steps:

- a) Laser light interaction - A laser beam is directed onto a sample. When the laser light interacts with the material, some of it gets scattered in different directions.
- b) Raman scattering - Most of the scattered light has the same energy as the incoming laser light, but a small portion of it undergoes a change in energy due to interactions with the molecules in the sample. This energy shift is known as the Raman scattering.
- c) Spectral analysis - The scattered light is collected and analysed using a spectrometer. The resulting Raman spectrum displays peaks and valleys that correspond to the vibrational modes of the molecules in the sample.
- d) Interpretation - Different molecules have distinct vibrational frequencies, which are captured as peaks in the spectrum. By comparing these peaks to known patterns, researchers can identify the chemical composition and structural characteristics of the material. [39]

ii) SEM (Scanning electron microscope)

SEM was first introduced in Cambridge university in 1965. Scanning Electron Microscopy (SEM) is a powerful imaging technique that helps to examine the surface morphology and microstructure of materials at high magnification. It provides detailed and three-dimensional images of samples by scanning them with a focused beam of electrons. SEM is widely used in

various scientific disciplines to study the structure, composition, and characteristics of different materials.

In SEM:

- a) **Electron Beam Interaction:** A focused beam of electrons is scanned over the sample's surface. When the electrons interact with the atoms on the sample's surface, various signals are emitted.
- b) **Secondary Electron Imaging:** One of the signals emitted is secondary electrons. These electrons are collected to create detailed images of the sample's surface. Secondary electron images provide information about the sample's topography, revealing features such as texture, roughness, and surface irregularities.
- c) **Backscattered Electron Imaging:** Another signal emitted is backscattered electrons. These electrons provide information about the sample's composition. Different elements have varying abilities to scatter electrons, resulting in differences in image contrast. This can help distinguish between materials with different atomic compositions.
- d) **Energy Dispersive X-ray Spectroscopy (EDS/EDX):** In conjunction with SEM, EDS is often used to analyse the chemical composition of the sample. EDS detects characteristic X-rays emitted by the sample when it's bombarded by the electron beam. This information can be used to identify the elements present in the sample and their relative concentrations.[39, 45, 46]

## 7. Results and discussion.

The flow diagram showing different phases of the preparation of the SiNP@graphene shell/GNS is shown in figure 4. A thin layer of silica is created on the surface of tiny silicon particles by reacting triethoxysilane (TES) with water. Then, a part of a molecule with a positive charge, (3-Aminopropyl)trimethoxysilane also known as KH550, sticks to the surface of these silicon-coated particles. This charged part is attracted to graphene oxide, which has some specific oxygen and hydrogen groups on its surface. This makes the graphene oxide molecules gather around the silicon-coated particles in a specific arrangement.

Next, everything is heated to a very high temperature of 500°C for 2 hours. At this high temperature, the graphene oxide changes and becomes a reduced form of graphene. Also, the silica layer on the silicon particles is removed during this heating process. As a result, the silicon particles covered by graphene form a unique structure that looks like a cage.

During all of this, the arrangement of the graphene layers stays the same. This means that when the cage structure forms, there's no need to add more graphene to make everything

stick together well. This way of making the samples are relatively simple and doesn't require complicated steps like electrospinning, pan fibre stabilization.[4] [40]

The sample was evaluated through SEM imaging and the results are shown in figure 14 & 15:

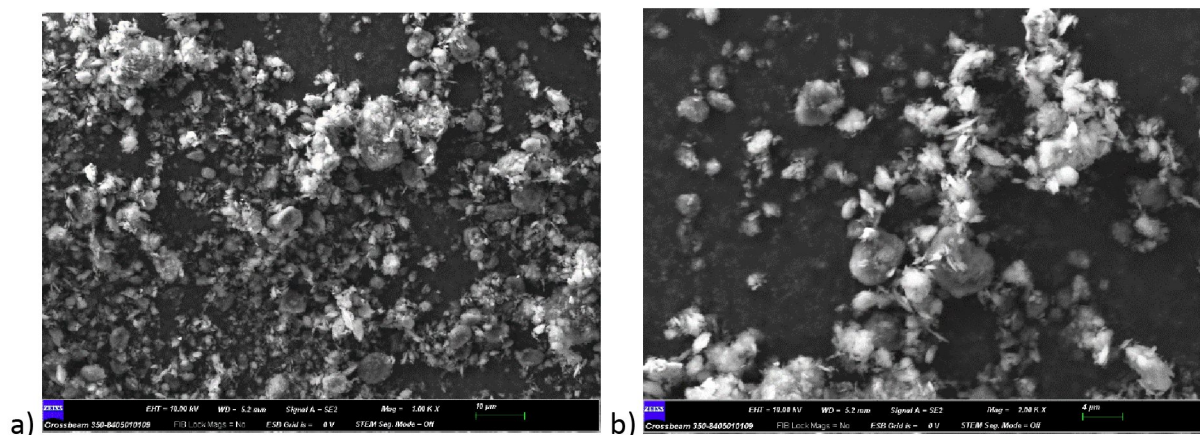


Figure 14 a) SEM imaging of SiNP@graphene shell/GNS at magnification of  $10\mu\text{m}$  b) SEM imaging of SiNP@graphene shell/GNS at magnification of  $4\mu\text{m}$ . Parameters set: EHT = 10 kV, WD = 5.2 mm, Signal A = SE2, FIB lock mags = No, ESB Grid is = No and STEM Seg. Mode = off.

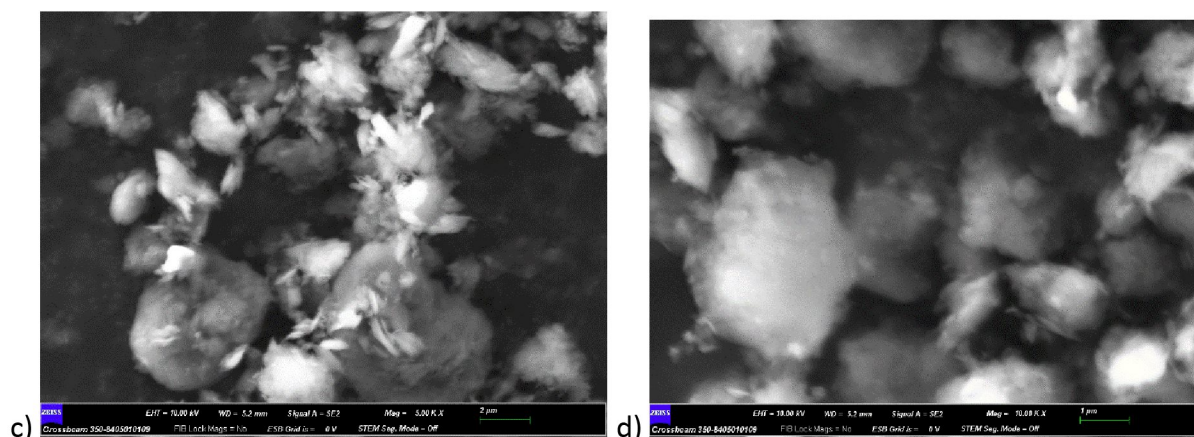


Figure 15 a) Magnified SEM imaging at  $2\mu\text{m}$  b) SEM imaging of SiNP@graphene shell/GNS at  $1\mu\text{m}$ . Parameters set: EHT = 10 kV, WD = 5.2 mm, Signal A = SE2, FIB lock mags = No, ESB Grid is = No and STEM Seg. Mode = off.

The images shown in figure 14 & 15 depicts the SEM imaging of sample obtained from silicon nanoparticles. Figure 14 a) shows the consistency of the reduced Si NP with graphene caging which is visible in figure 15 b) under magnification of  $1\mu\text{m}$ . As the magnification increases, we can see the smoothness of the Si NP with graphene caging however the trace of graphene nanosheet on which all the graphene caged Si NP are supposed to be anchored is missing as shown in figure 4.

The formation of graphene caged Si NP shows that the calcination and etching process gave the desired result by reducing the GO and etching away of silica layer, but the missing GNS shows that the electrostatic self-assembly part was accomplished only partially as the positive part KH550 did assemble itself over Si NP and formed a bond with GO particles but failed to have it anchored on GNS.

This can also be explained through the EDX results. Figure 16 shows the region spectrum which was analysed for chemical composition of the sample.

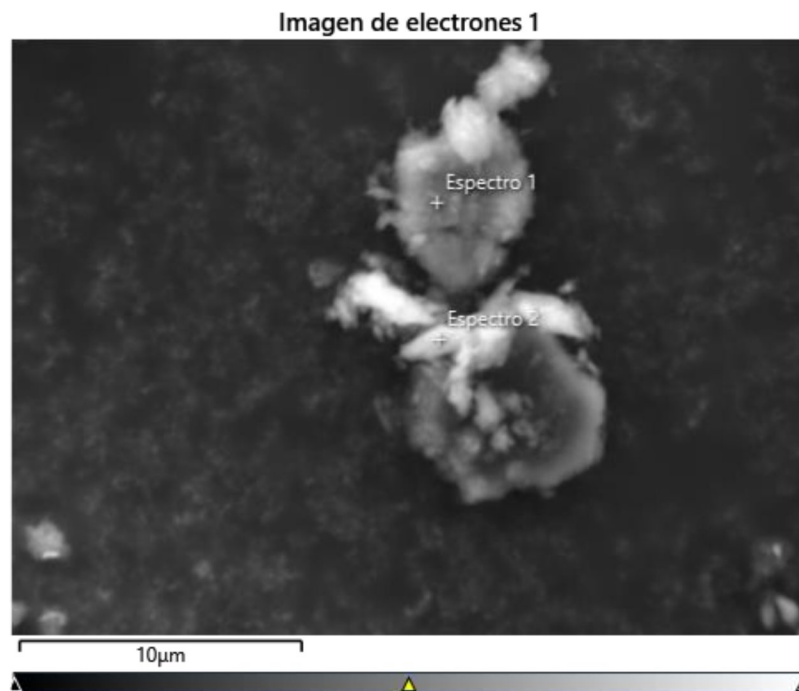


Figure 16 – Shows the spectrum 1 and 2 analysed under EDX for material composition at magnification scale of 10µm.

The result for spectrum 1 is shown in graph in figure 17.

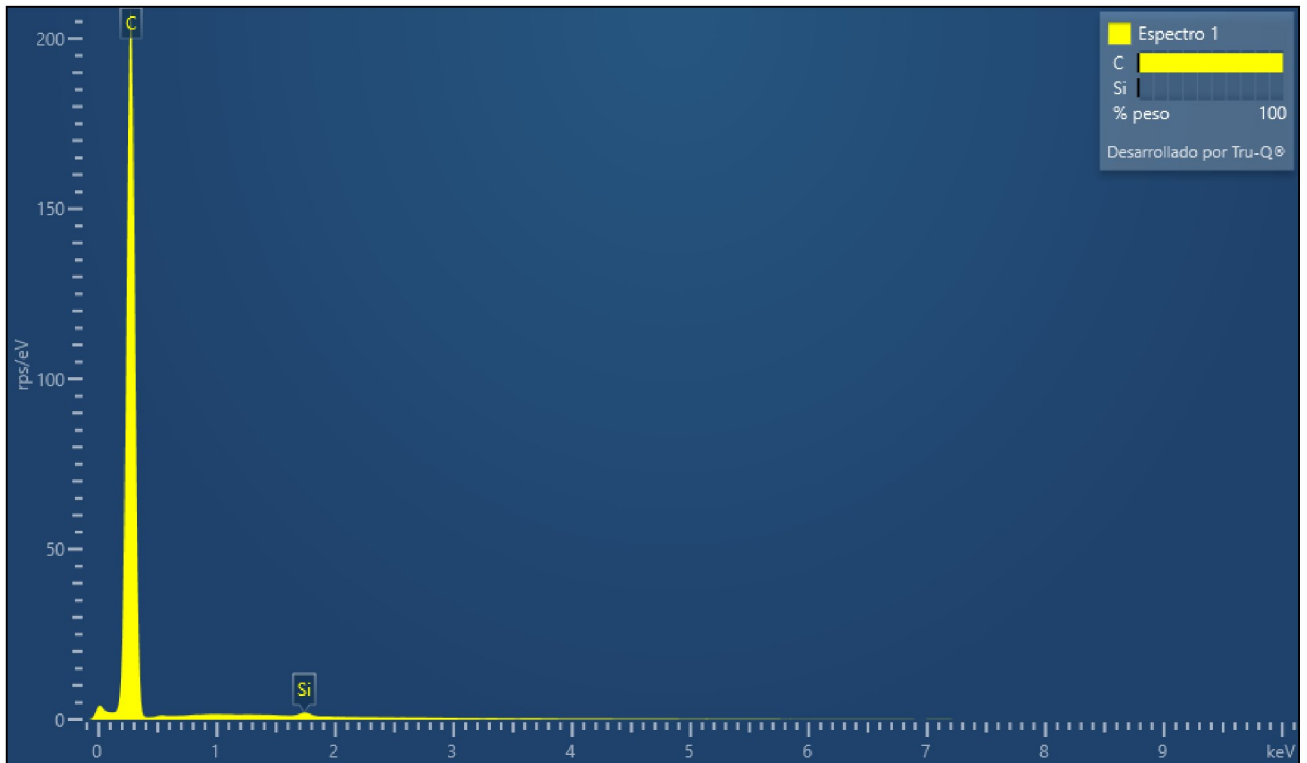


Figure 17 – material composition for spectrum 1.

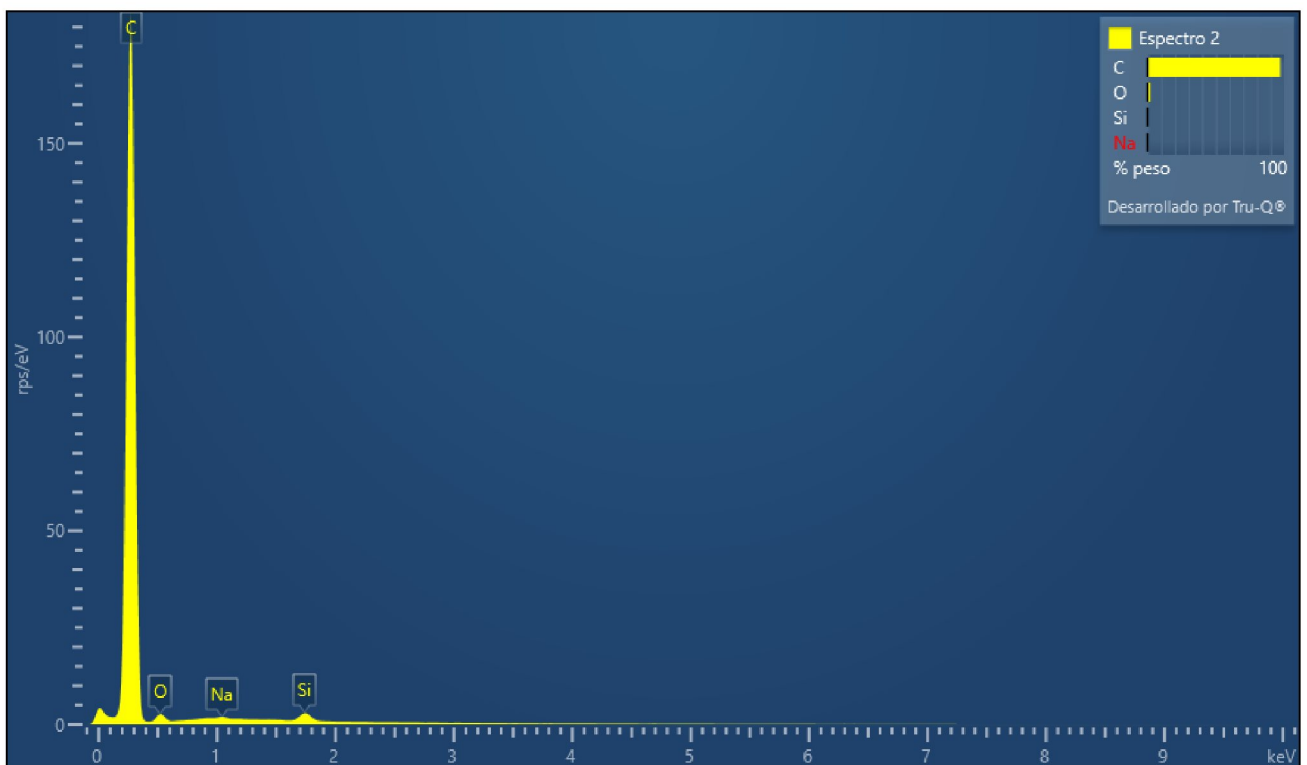


Figure 18 – material composition for spectrum 2.

In figure 17 and 18 it illustrates that the weight percentage of carbon is very high as compared to Silicon and there are some percentages of oxygen and sodium as well which is inconsistent as it is only traced in spectrum 2 and not 1. The high percentage of carbon tells that the

addition of GO was in disproportionate amount and probably that is the reason for Si NP in GO shell not anchored with GNS. Also, the presence of oxygen can result in still some presence of  $\text{SiO}_2$  which also shows in the FTIR result in figure 19. The pointy part at  $1066 \text{ cm}^{-1}$  confirms the GO spectrum marked in red in figure 19. This pointy part comes from the stretching of carbon oxygen atoms in the GO [47]. Similarly, the peak at  $1085 \text{ cm}^{-1}$  marked in blue in figure 18 are related to the stretching, bending, and tilting of the bonds between silicon and oxygen atoms in the material confirms the presence of  $\text{SiO}_2$ . Also, the peak in the area  $1600 \text{ cm}^{-1}$  and  $2300 \text{ cm}^{-1}$  in the spectrum shows the presence of carbon impurities shown as black marked are in the figure 19 [48].

The SiNP@graphene cage/GNS was further analysed by Raman measurement as shown in figure 20, the peak around  $514 \text{ cm}^{-1}$  which is produced by Silicon is weaker whereas a strong peak is formed near  $1350 \text{ cm}^{-1}$  and relatively weaker peak formed at  $1572 \text{ cm}^{-1}$  corresponds to D & G band of graphene. The D band comes from imperfections in the carbon atom, which indicates the material's irregularities[49]. On the other hand, the G band arises from the stretching movement of the C atom's  $\text{sp}^2$  hybridization [4, 50]. Other than that, the peak at  $1118 \text{ cm}^{-1}$  depicts C-N stretching [51] and peak at  $2678 \text{ cm}^{-1}$  assigns to 2D band CNT [52].

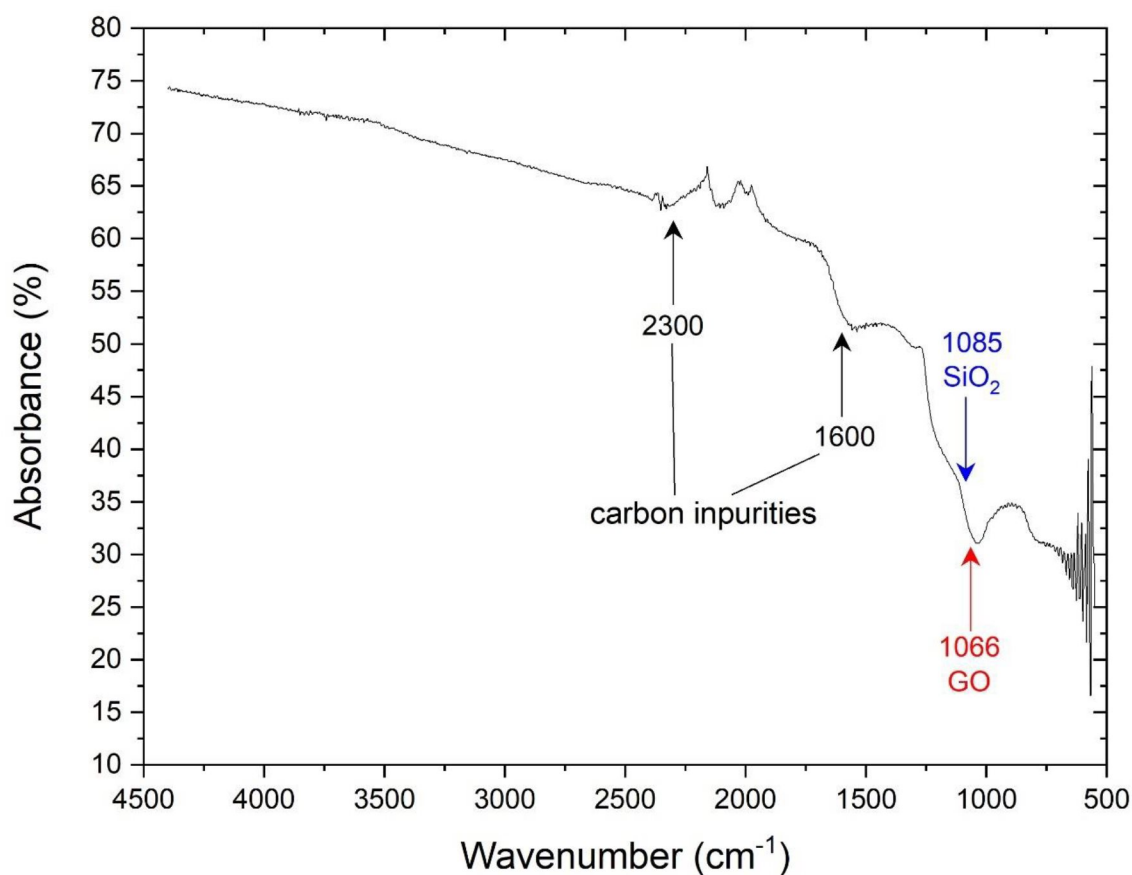


Figure 19 – The FTIR result of the Si@SiO<sub>2</sub>@GNS before calcination.

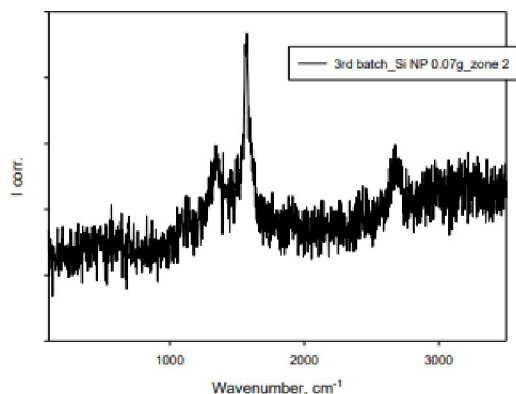


Figure 20 – Raman spectrum of SiNP@graphene cage/GNS.

The outcomes were quite similar when we compare to a sample consisting of silicon microparticles (with a mesh size of 325) under the SEM, as we can see in Figure 21. However, the consistency of how the graphene forms a protective structure around these silicon microparticles isn't as smooth. In Figure 21a, where the magnification is of 20 $\mu$ m, it is similar to what we observed in the silicon nanoparticles shown in Figure 14(a) – the graphene nanosheets (GNS) are missing. But, when we increase the magnification to observe how the graphene encases the silicon microparticles, the surface does not appear as smooth as it did with the silicon nanoparticles. This difference might be due to the size of the silicon microparticles, which gives a larger surface area for the graphene oxide (GO) to wrap around. This uneven coverage of GO over the silicon microparticles might not provide enough space for the microparticles to expand during the process of lithiation. This could lead to the pulverization of microparticles, causing the battery's capacity to decrease rapidly. As a result, the battery's lifespan might be affected, leading to fewer charge and discharge cycles.

The comparison of Si NP and microparticles at 1  $\mu$ m magnification in SEM imaging is shown on figure 22. It is quite clear that Si NP a) has much better surface consistency of graphene oxide as compared to Si microparticles in b). The caging of Si particles by GO is much even with NP. With microparticles since the surface area is much larger, the consistency of encasing of GO is compromised. Thus, according to this characterization of the materials Si NP is preferred over microparticles for making the anode.

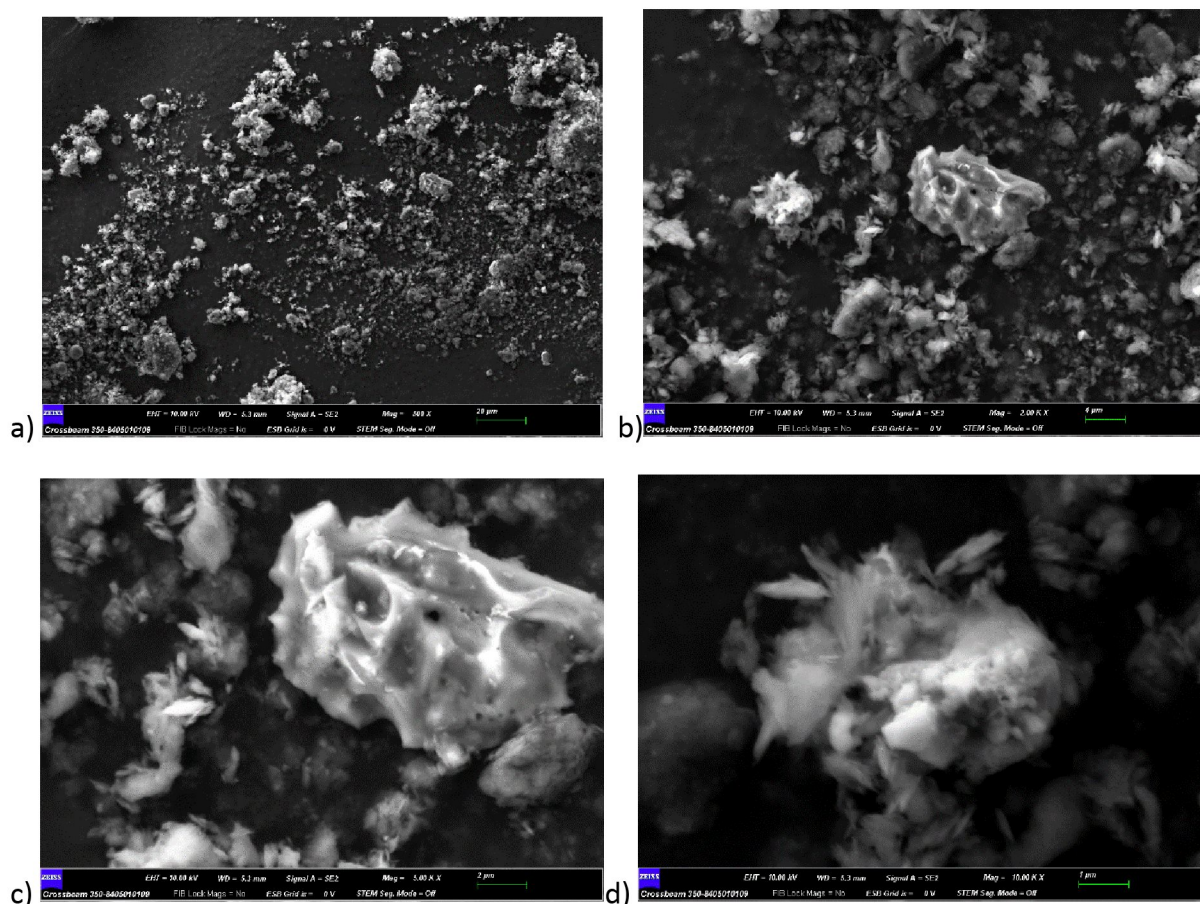


Figure 21 – The SEM imaging of Si microparticles(325Mesh) a) with magnification of 20 $\mu$ m b) with magnification of 4 $\mu$ m c) with magnification of 2 $\mu$ m d) with magnification of 1 $\mu$ m.

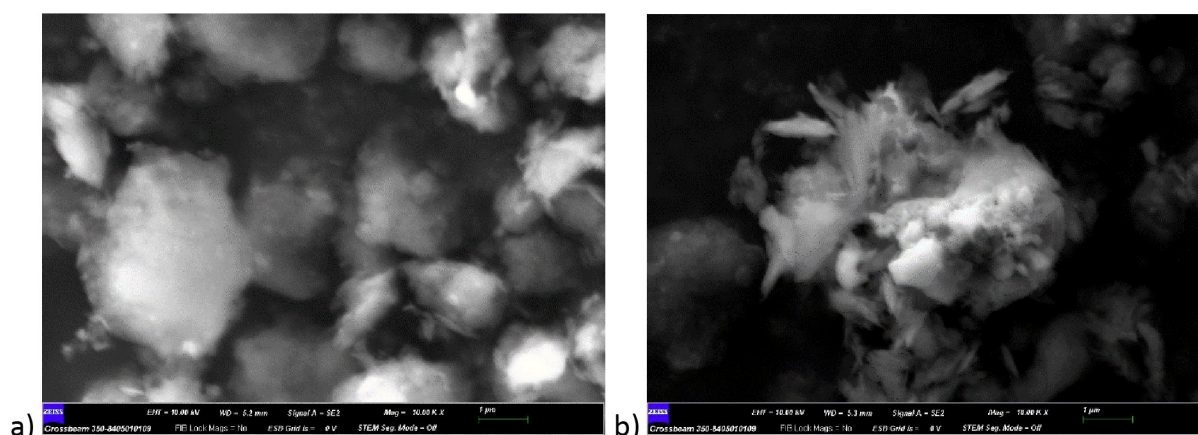


Figure 22 – Comparison of Si NP and microparticle in 1 $\mu$ m magnification a) Si nanoparticles b) Si microparticles.

As we have seen so far, the material characteristic of SiNP@graphene cage/GNS was not observed as expected and the same happened with the electrochemical tests as well. The assembled full cell was tested on testing unit -CT-4008T-5V10mA-164 from Neware in a voltage window of 1-2 V at 100 mA $g^{-1}$ . Figure 23 shows the curve of 1<sup>st</sup>, 10<sup>th</sup>, 50<sup>th</sup> & 100<sup>th</sup> charge discharge cycles. The charge discharge test is used to evaluate the performance and durability of rechargeable batteries over multiple charging and discharging cycles.

From the graph in figure 23, It is obvious that the first charge cycle showed specific capacity of 315 mAh/g, which immediately drops to 3 mAh/g and after that it keeps on reducing to around 2 mAh/g which is impractical for a performance of cell, also shown in figure 24. In a LIB made of silicon and carbon composite anode the specific capacity has been achieved as high as 929 mAh/g after 50 cycles [40] and also over 1500 mAh/g after 100 cycles [4].

After the first charge cycle in the graph in figure 23 the other charge cycles starts to get charged from 1.2 V and goes till 2 V and discharge cycles starts to get discharged from 1.7 V and discharges till 1 V which is a very unusual pattern because it expected to start charging at 1V and charge till 2V and vice versa for discharge cycle. For every charge and discharge cycle there is a lag of 0.3 V. Even the first charge cycle which has attained the maximum capacity is no way near to the expected mark of over 1000 mAh/g. Another point to note here is that, in the discharge cycles there shows a rapid slope between 1.5 to 1.1 V pointing to the formation of SEI layer but this cannot be confirmed either, looking at the performance of the cell.

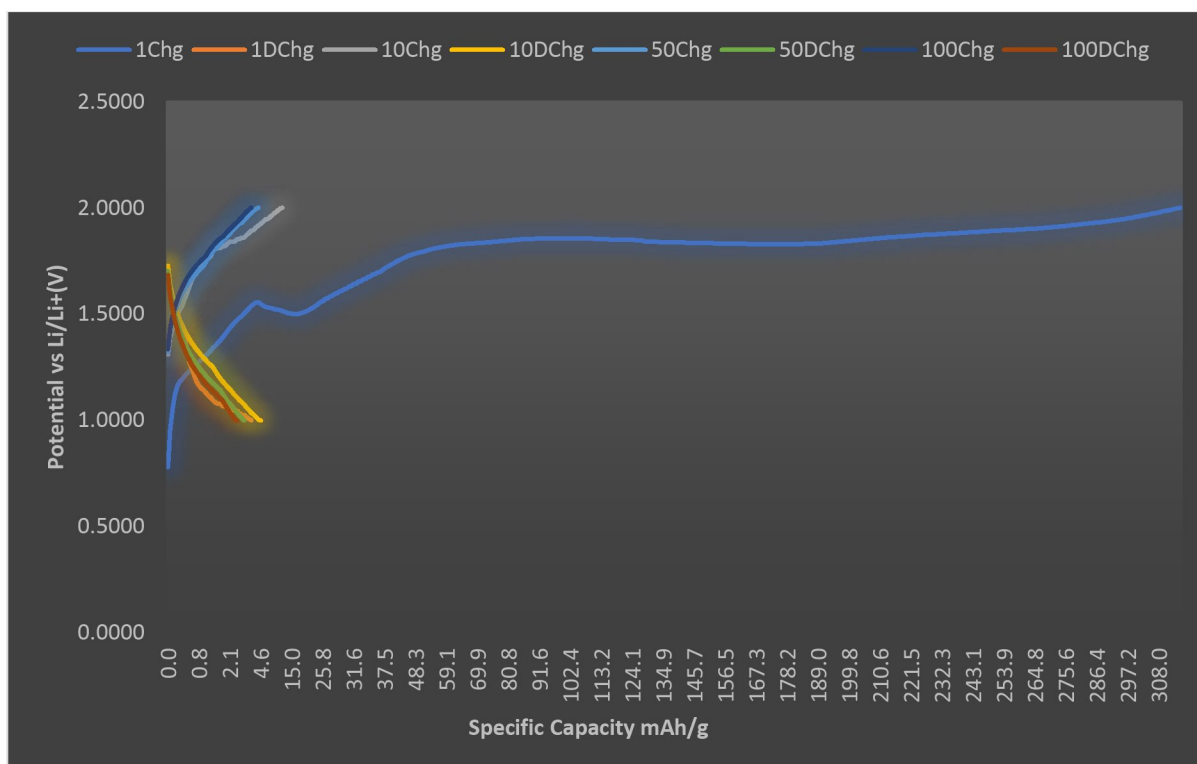


Figure 23 – Initial charge discharge curve of SiNP@graphene cage/GNS.

In the performance graph in figure 24 shows the rapid deterioration of specific capacity after first charge cycle, which is most likely to happen because of the pulverization. Which means that the objective of overcoming the pulverization – with the use of nano Si and carbon composite was never achieved, which shows from the material characterization as well. Towards the 100<sup>th</sup> cycle the specific capacity curve is almost touching 0 line making the cell dysfunctional.

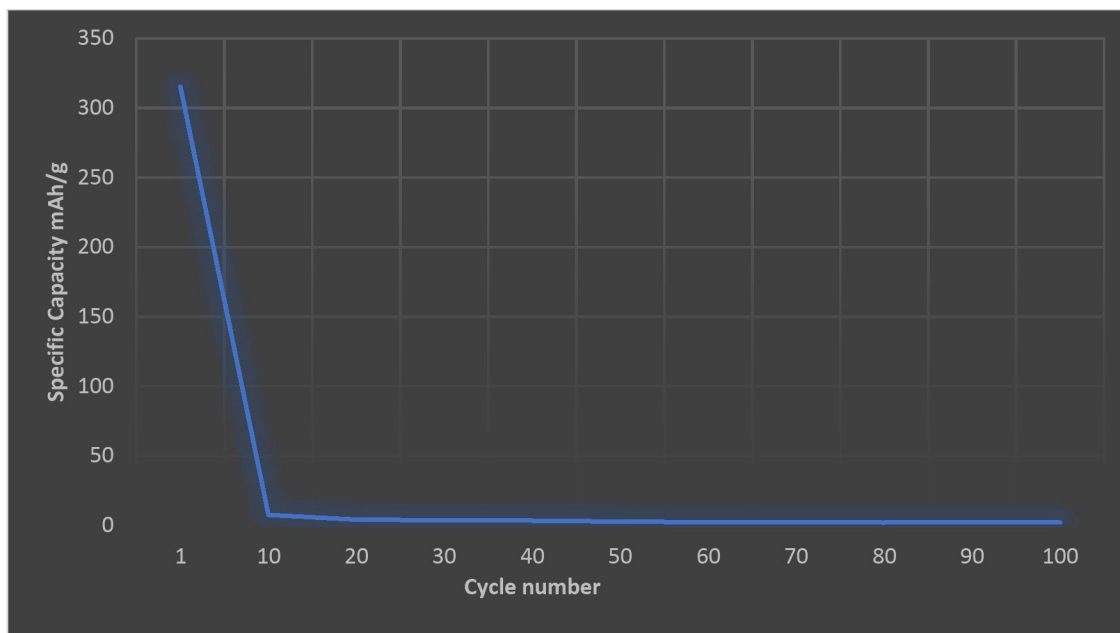


Figure 24 – Cycling performance of SiNP@graphene cage/GNS

Figure 25 shows the coulombic efficiency with cycle number. The efficiency dwells between 40 to 50% over 100 charge discharge cycles. The 1st cycle has an efficiency of almost 1% and increase rapidly till 20th cycle showing the formation of SEI layer which stabilizes after first 20 cycles. The coulombic efficiency is defined as the ratio of specific capacity achieved during discharge and charge cycle, but the charge discharge cycle of the dysfunctional cell shows the same curve with almost dead specific capacity that is why the efficiency curve seems to be stabilizing after 60 cycles.

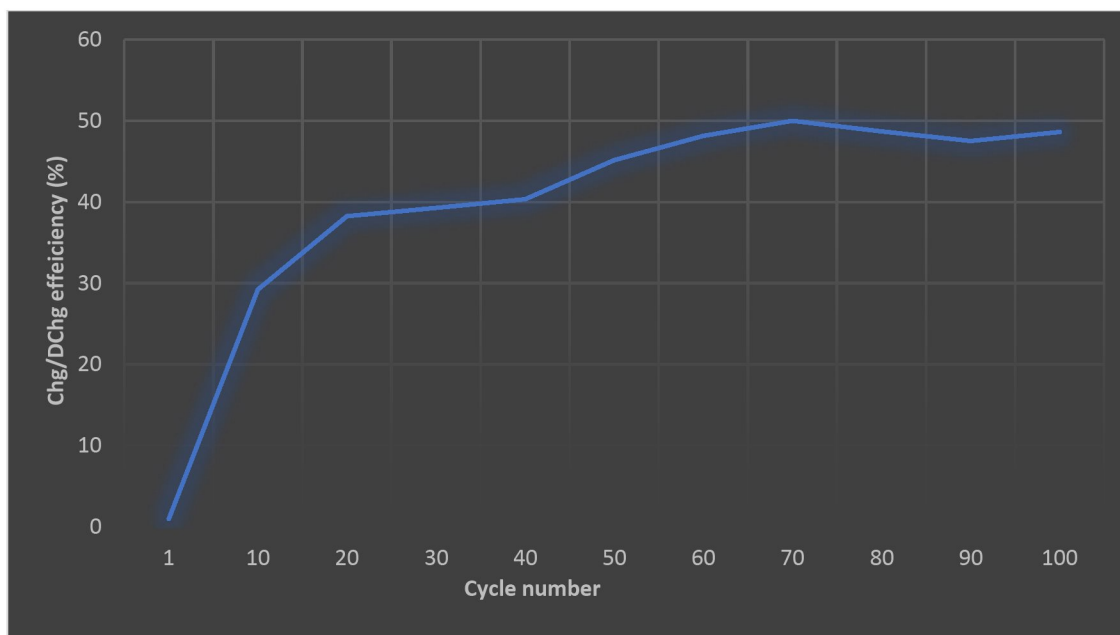


Figure 25 – Charge discharge cycle efficiency of SiNP@graphene cage/GNS.

## 8. Conclusion.

The research was conducted with an objective of using Silicon nanoparticles to avoid the pulverization, which is the major challenge stopping the application of Silicon as anode material, but the objective was clearly not achieved with the results received from the material and electrochemical tests. The experimental technique used in this experiment has drawbacks like disproportionate use of GO, improper calcination, and cell assembly. The presence of oxygen also suggests that the process like calcination and cell assembly requires inert atmosphere. The presence of carbon increases the ion mobility making the anode structure conductive but since the GNS was missing the drop of specific capacity is obvious also the low specific capacity suggests that the coin cell assembly process must be improved to avoid any short circuiting.

In summary, this experimental procedure to make anode from Si NP and GO should be performed again with more suitable concentration of GO. This can be achieved by performing the repetitive chemical characterization of sample until the desired morphology is achieved. The sample must undergo calcination at a high temperature such as 700°C under inert atmosphere to avoid the presence of oxygen which reacts to form silica  $\text{SiO}_2$ . Assembly of the cell is a critical part of the whole procedure; it is important to make sure that the electrodes are placed at the centre of the cell and the amount of electrolyte is as per the gauge. There are several small but important steps like using plastic tweezers to avoid the short circuiting of cell, keeping electrolyte in a dark container – that should be taken care of. The assembly of the cell should be done in a proper inert atmosphere to avoid any side reactions in the electrode due to the presence of oxygen. The anode making technique used in this research is simple and has a promising result prospect according to the theory, but it is critical to find the right composition and more controlled experimental environment. Thus, it is recommended to use this technique with suggested precautions to get the optimum result which will certainly boost the development of more improved and efficient LIBs.

## 9. Reference.

1. Kiehne, H.A., *Battery technology handbook*. Vol. 118. 2003: CRC Press.
2. *Electrochemical Cells*.
3. Franco Gonzalez, A., N.-H. Yang, and R.-S. Liu, *Silicon Anode Design for Lithium-Ion Batteries: Progress and Perspectives*. The Journal of Physical Chemistry C, 2017. **121**(50): p. 27775-27787.
4. Han, X.-Y., et al., *Graphene caging silicon nanoparticles anchored on graphene sheets for high performance Li-ion batteries*. Applied Surface Science, 2019. **484**: p. 11-20.
5. Wu, H., et al., *Stable Li-ion battery anodes by in-situ polymerization of conducting hydrogel to conformally coat silicon nanoparticles*. Nature Communications, 2013. **4**(1): p. 1943.
6. Jin, Y., et al., *Challenges and Recent Progress in the Development of Si Anodes for Lithium-Ion Battery*. Advanced Energy Materials, 2017. **7**(23): p. 1700715.
7. Li, X., et al., *Mesoporous silicon sponge as an anti-pulverization structure for high-performance lithium-ion battery anodes*. Nature Communications, 2014. **5**(1): p. 4105.
8. Sun, L., et al., *Recent progress and future perspective on practical silicon anode-based lithium ion batteries*. Energy Storage Materials, 2022. **46**: p. 482-502.
9. Zang, J.-L. and Y.-P. Zhao, *Silicon nanowire reinforced by single-walled carbon nanotube and its applications to anti-pulverization electrode in lithium ion battery*. Composites Part B: Engineering, 2012. **43**(1): p. 76-82.
10. Yu, W.-J., et al., *Lithiation of Silicon Nanoparticles Confined in Carbon Nanotubes*. ACS Nano, 2015. **9**(5): p. 5063-5071.
11. Yoon, D.-E., et al., *Dependency of Electrochemical Performances of Silicon Lithium-Ion Batteries on Glycosidic Linkages of Polysaccharide Binders*. ACS Applied Materials & Interfaces, 2016. **8**(6): p. 4042-4047.
12. Guan, X., et al., *Metal-Chelated Biomimetic Polyelectrolyte as a Powerful Binder for High-Performance Micron Silicon Anodes*. Energy Technology, 2020. **8**(7): p. 2000278.
13. Heiskanen, S.K., J. Kim, and B.L. Lucht, *Generation and Evolution of the Solid Electrolyte Interphase of Lithium-Ion Batteries*. Joule, 2019. **3**(10): p. 2322-2333.
14. Xiao, Z., et al., *Research progress of nano-silicon-based materials and silicon-carbon composite anode materials for lithium-ion batteries*. Journal of Solid State Electrochemistry, 2022. **26**(5): p. 1125-1136.
15. Wu, H., et al., *Stable cycling of double-walled silicon nanotube battery anodes through solid-electrolyte interphase control*. Nature Nanotechnology, 2012. **7**(5): p. 310-315.
16. Hsu, Y.-C., C.-C. Hsieh, and W.-R. Liu, *Synthesis of double core-shell carbon/silicon/graphite composite anode materials for lithium-ion batteries*. Surface and Coatings Technology, 2020. **387**: p. 125528.
17. Shen, X., et al., *Research progress on silicon/carbon composite anode materials for lithium-ion battery*. Journal of Energy Chemistry, 2018. **27**(4): p. 1067-1090.
18. Lai, S.-C., *Solid lithium-silicon electrode*. Journal of the Electrochemical Society, 1976. **123**: p. 1196.
19. Seefurth, R.N. and R.A. Sharma, *Investigation of Lithium Utilization from A Lithium-Silicon Electrode*. Journal of The Electrochemical Society, 1977. **124**(8): p. 1207.
20. Boukamp, B.A., G.C. Lesh, and R.A. Huggins, *All-Solid Lithium Electrodes with Mixed-Conductor Matrix*. Journal of The Electrochemical Society, 1981. **128**(4): p. 725.
21. A. M. Wilson, B.M.W., and J. R. Dahn, *Nanodispersed silicon in pregraphitic carbons*. 1995.
22. Li, H., et al., *A High Capacity Nano - Si Composite Anode Material for Lithium Rechargeable Batteries*. Electrochemical and Solid-State Letters, 1999. **2**(11): p. 547.
23. Wen, Z.S., et al., *High capacity silicon/carbon composite anode materials for lithium ion batteries*. Electrochemistry Communications, 2003. **5**(2): p. 165-168.

24. Liu, Y., et al., *Silicon/carbon composites as anode materials for Li-ion batteries*. Electrochemical and solid-state letters, 2004. **7**(10): p. A369.
25. Zuo, P., G. Yin, and Y. Ma, *Electrochemical stability of silicon/carbon composite anode for lithium ion batteries*. Electrochimica Acta, 2007. **52**(15): p. 4878-4883.
26. Kim, H. and J. Cho, *Superior Lithium Electroactive Mesoporous Si@Carbon Core-Shell Nanowires for Lithium Battery Anode Material*. Nano Letters, 2008. **8**(11): p. 3688-3691.
27. Xu, Y., et al., *Nanosized core/shell silicon@ carbon anode material for lithium ion batteries with polyvinylidene fluoride as carbon source*. Journal of Materials Chemistry, 2010. **20**(16): p. 3216-3220.
28. Rand, B., *Calcination*, in *Concise Encyclopedia of Advanced Ceramic Materials*, R.J. Brook, Editor. 1991, Pergamon: Oxford. p. 49-51.
29. Kaur, B. and S.N. Bhattacharya, *7 - Automotive dyes and pigments*, in *Handbook of Textile and Industrial Dyeing*, M. Clark, Editor. 2011, Woodhead Publishing. p. 231-251.
30. Kumar, J., S. Mandal, and N. Mahato, *Study of Electro Chemical Machining Etching Effect on Surface Roughness and Variation with Chemical Etching Process*. 2019.
31. Liu, C.-P., et al., *Facile chemical method of etching polyimide films for failure analysis (FA) applications and its etching mechanism studies*. Microelectronics Reliability, 2014. **54**(5): p. 911-920.
32. Arora, P. and Z. Zhang, *Battery Separators*. Chemical Reviews, 2004. **104**(10): p. 4419-4462.
33. Kim, Y., et al., *Investigation of mass loading of cathode materials for high energy lithium-ion batteries*. Electrochemistry Communications, 2023. **147**: p. 107437.
34. Qian, J., et al., *Electrochemical surface passivation of LiCoO<sub>2</sub> particles at ultrahigh voltage and its applications in lithium-based batteries*. Nature Communications, 2018. **9**(1): p. 4918.
35. Siczek, K.J., *Chapter Eight - Negative Electrode (Anode) Materials*, in *Next-Generation Batteries with Sulfur Cathodes*, K.J. Siczek, Editor. 2019, Academic Press. p. 117-131.
36. Murray, V., D.S. Hall, and J.R. Dahn, *A Guide to Full Coin Cell Making for Academic Researchers*. Journal of The Electrochemical Society, 2019. **166**(2): p. A329.
37. Nölle, R., et al., *A reality check and tutorial on electrochemical characterization of battery cell materials: How to choose the appropriate cell setup*. Materials Today, 2020. **32**: p. 131-146.
38. Qi, Z., H. Dong, and G.M. Koenig, *Electrochemical Characterization of Lithium-Ion Battery Cathode Materials with Aqueous Flowing Dispersions*. Electrochimica Acta, 2017. **253**: p. 163-170.
39. Liu, X., et al., *Advanced material characterization techniques for sodium-ion battery*. Asia-Pacific Journal of Chemical Engineering, 2022. **17**(4): p. e2800.
40. Yan, Y., et al., *Electrospinning-Enabled Si/C Nanofibers with Dual Modification as Anode Materials for High-Performance Lithium-Ion Batteries*. Acta Metallurgica Sinica (English Letters), 2021. **34**(3): p. 329-336.
41. Bensalah, N., et al., *Silicon nanofilms as anode materials for flexible lithium ion batteries*. Thin Solid Films, 2019. **690**: p. 137516.
42. Gandomi, Y.A., et al., *Critical Review—Experimental Diagnostics and Material Characterization Techniques Used on Redox Flow Batteries*. Journal of The Electrochemical Society, 2018. **165**(5): p. A970.
43. Xie, Y., J. Li, and C. Yuan, *Mathematical modeling of the electrochemical impedance spectroscopy in lithium ion battery cycling*. Electrochimica Acta, 2014. **127**: p. 266-275.
44. Lu, J., T. Wu, and K. Amine, *State-of-the-art characterization techniques for advanced lithium-ion batteries*. Nature Energy, 2017. **2**(3): p. 17011.
45. Ge, M., et al., *Deep learning analysis on microscopic imaging in materials science*. Materials Today Nano, 2020. **11**: p. 100087.
46. Azad MOHAMMED, A.A., *SCANNING ELECTRON MICROSCOPY (SEM): A REVIEW*. 2018.
47. Andrijanto, E., et al., *Facile synthesis of graphene from graphite using ascorbic acid as reducing agent*. Vol. 1725. 2016. 020003.

48. Shokri, B., M. Abbasi-Firouzjah, and S.I. Hosseini, *FTIR analysis of silicon dioxide thin film deposited by Metal organic-based PECVD*. Proceedings of 19th International Symposium on Plasma Chemistry Society, 2009.
49. Nie, P., et al., *Graphene Caging Silicon Particles for High-Performance Lithium-Ion Batteries*. *Small*, 2018. **14**(25): p. 1800635.
50. Zhang, Y., et al., *Self-templated Synthesis of Nickel Silicate Hydroxide/Reduced Graphene Oxide Composite Hollow Microspheres as Highly Stable Supercapacitor Electrode Material*. *Nanoscale Research Letters*, 2017. **12**(1): p. 325.
51. Pezzotti, G., *Raman spectroscopy in cell biology and microbiology*. *Journal of Raman Spectroscopy*, 2021. **52**(12): p. 2348-2443.
52. Isaac Childres, L.A.J., c, Wonjun Park<sup>b,c</sup>, Helin Cao<sup>a,b</sup> and Yong P. Chen<sup>a,b,c</sup>, *RAMAN SPECTROSCOPY OF GRAPHENE AND RELATED MATERIALS*.